ELEMENTA
Science of the Anthropocene

Klausner, T, et al. 2020. Urban greenhouse gas emissions from the Berlin area: A case study using airborne CO_2 and CH_4 in situ observations in summer 2018. *Elem Sci Anth,* 8: 15. DOI: https://doi.org/10.1525/elementa.411

RESEARCH ARTICLE

Urban greenhouse gas emissions from the Berlin area: A case study using airborne CO_2 and CH_4 in situ observations in summer 2018

T. Klausner*, M. Mertens*, H. Huntrieser*, M. Galkowski†,‡, G. Kuhlmann§, R. Baumann*, A. Fiehn*, P. Jöckel*, M. Pühl* and A. Roiger*

Urban areas are recognised as a significant source of greenhouse gas emissions (GHG), such as carbon dioxide (CO_2) and methane (CH_4). The total amount of urban GHG emissions, especially for CH_4, however, is not well quantified. Here we report on airborne in situ measurements using a Picarro G1301-m analyser aboard the DLR Cessna Grand Caravan to study GHG emissions downwind of the German capital Berlin. In total, five aircraft-based mass balance experiments were conducted in July 2018 within the Urban Climate Under Change [UC]^2 project. The detection and isolation of the Berlin plume was often challenging because of comparatively small GHG signals above variable atmospheric background concentrations. However, on July 20th enhancements of up to 4 ppm CO_2 and 21 ppb CH_4 were observed over a horizontal extent of roughly 45 to 65 km downwind of Berlin. These enhanced mixing ratios are clearly distinguishable from the background and can partly be assigned to city emissions. The estimated CO_2 emission flux of 1.39 ± 0.76 t s^{-1} is in agreement with current inventories, while the CH_4 emission flux of 5.20 ± 1.70 kg s^{-1} is almost two times larger than the highest reported value in the inventories. We localized the source area with HYSPLIT trajectory calculations and the global/regional nested chemistry climate model MECO(n) (down to ~1 km), and investigated the contribution from sewage-treatment plants and waste deposition to CH_4, which are treated differently by the emission inventories. Our work highlights the importance of strong CH_4 sources in the vicinity of Berlin and shows, that there is limited understanding of CH_4 emissions from urban regions, even for major cities in highly developed countries like Germany. Furthermore, we show that a detailed knowledge of GHG inflow mixing ratios is necessary to suitably estimate emission rates for Berlin.

Keywords: Urban; Greenhouse gas; Carbon dioxide; Methane; Airborne mass balance approach; In-situ

1 Introduction

Atmospheric mixing ratios of well-known greenhouse gases (GHGs), such as carbon dioxide (CO_2) and methane (CH_4), have increased by a factor of 1.4 and 2.5, respectively, compared to pre-industrial times (Hartmann et al., 2013). These gases contribute substantially to global warming due to the increased absorption of outgoing infrared radiation. The Paris Agreement (UNFCCC, 2015) aims to keep the global temperature rise below 2°C compared to pre-industrial levels. To achieve this ambitious goal, GHG emissions have to be reduced. However, for the development of efficient mitigation strategies and for the prediction of future climate impacts, an improved understanding and quantification of the GHG budget is needed. Typically two different approaches are used to estimate emissions.

The bottom-up approach has the advantage that emissions can be calculated globally and sector-wise. Furthermore, it provides detailed information about the different emission processes, but relies on statistical activity data and emission factors. It is well known that such input data are subject to large spatial and temporal heterogeneity, as well as to simplified assumptions with large uncertainties (Nisbet and Weiss, 2010; Brandt et al., 2014). The so-called top-down approach is based on atmospheric observations (on different scales), which are used to derive emission rates either with a mass-balance approach, as done in this study, or with inverse modelling techniques. These emission rates are commonly used to independently validate total bottom-up emissions, while the source

* Deutsches Zentrum für Luft- und Raumfahrt (DLR), Institut für Physik der Atmosphäre, Oberpfaffenhofen, DE

† Max-Planck-Institut für Biogeochemie (MPI), Biogeochemische Systeme (BGC), Jena, DE

‡ AGH University of Science and Technology, Faculty of Physics and Applied Computer Science, Kraków, PL

§ Empa, Swiss Federal Laboratories for Materials Science and Technology, Dübendorf, CH

Corresponding author: T. Klausner (theresa.klausner@dlr.de)

attribution to different emission processes usually is more challenging. Estimating emissions with bottom-up and top-down approaches can either provide insight into large discrepancies (as shown e.g. by an ensemble of seven different inverse models estimating ~30% higher European CH_4 emissions than bottom-up reported values (Bergamaschi et al., 2018)), or can confirm reported emissions (as shown e.g. for the city of Indianapolis by Turnbull et al. (2019)).

Currently urban areas cover less than 3% of the terrestrial earth's surface (Liu et al., 2014), but accommodate more than half of the world's population, with a persistently increasing trend (UN, 2018). This spatial concentration of human activities and their high energy consumption make cities a hotspot for GHG emissions (Kennedy et al., 2012; Marcotullio et al., 2013). With respect to CH_4, global anthropogenic emissions are relatively well-known, but the contributions of single source sectors on the national, regional and city scale are often not well quantified (Kirschke et al., 2013; Saunois et al., 2017). Total CO_2 emissions of developed countries can be estimated with high accuracy (due to the precise knowledge of national fossil fuel consumption amounts), however, the spatial and temporal distribution of emissions is less well known because of lack of appropriate data (Bréon et al., 2015). Therefore, several observational studies have focused on estimating CH_4 and CO_2 emissions from urban areas. Based on airborne measurements a major source of elevated CH_4 from cities in the United States was attributed to emissions related to natural gas and landfills (e.g. Cambaliza et al., 2015; Ren et al., 2018; Plant et al., 2019). Airborne studies on European cities are relatively sparse. To the best of our knowledge, they have been conducted in London (O'Shea et al., 2014; Pitt et al., 2019) and Rome (Gioli et al., 2014). While airborne derived CO_2 emissions from Rome were found to agree with inventorial data (Gioli et al., 2014), CO_2 and CH_4 emissions from London need to be scaled by a factor of 1.57 and 0.7, respectively, in order to agree with the airborne derived fluxes from Pitt et al. (2019). In this estimate peri-urban emissions from the greater London area were taken into account, which downscales their previous estimate based on the conventional mass balance approach (factors of 3.08 for CO_2 and 1.22 for CH_4, given in the same study). Ground-based observations in London (Helfter et al., 2016), Paris (Bréon et al., 2015), Cracow (Kuc et al., 2003; Zimnoch et al., 2019) and Florence (Gioli et al., 2012) provide additional information on urban GHG emissions, e.g. long-term CO_2 observations in Florence indicate 19% higher emissions than reported by inventories (Gioli et al., 2012). Atmospheric monitoring sites in Paris, together with an atmospheric inversion approach, point towards an overestimation of urban emissions by the local inventory (Bréon et al., 2015).

Here we report on aircraft-based in situ measurements of atmospheric CH_4 and CO_2 mixing ratios in order to estimate GHG emissions of Berlin. Five research flights up- and downwind of Berlin were conducted in July 2018 with the DLR Cessna aircraft in the framework of the Urban Climate Under Change project [UC]^2 (Scherer et al., 2019b). Berlin itself is an interesting target for studying urban GHG emissions, as it is the largest German city in terms of area and second largest city in terms of population density (Statistisches Bundesamt, 2018). CO_2 emissions for the greater Berlin area (~33 Mt a^{-1}) are expected to be roughly similar to emissions from the well-studied London area (~32 Mt a^{-1}), while CH_4 emissions are ~50% lower (Berlin ~28 kt a^{-1}, London ~53 kt a^{-1}) when comparing estimates from Pitt et al. (2019) with the CAMS GHG inventory for 2015 (Kuenen et al., 2014). The relatively isolated location of Berlin and its flat topography makes the city an ideal target for the aircraft-based mass balance approach. To the best of our knowledge, the only published study on experimentally determined GHG fluxes from Berlin is by Hase et al. (2015) who estimated the CO_2 source strength of Berlin with ground-based Fourier-Transform infrared spectrometers. The city of Berlin has also been in the focus of several studies on the potential use of satellite measurements for estimating CO_2 emissions. They show, that even for future and highly sophisticated satellite systems, the identification and quantification of the Berlin city plume is extremely challenging (Pillai et al., 2016; Kuhlmann et al., 2019b), so that dedicated measurement campaigns will be an invaluable tool for validating both top-down and bottom-up inventories.

This paper is structured as follows: Section 2 introduces the aircraft instrumentation, the mass balance approach, the model setups, and compares three different emission inventories for the Berlin area. A mission overview is presented in Sect. 3.1. In Sect. 3.2 we assess the CO_2 and CH_4 emission rate for a selected flight on July 20th using the mass balance approach. We consider the history of the encountered air masses and discuss our estimate with respect to current GHG inventories. In Sect. 3.3 we compare our observations with simulated GHG mixing ratios from the global/regional nested chemistry climate model MECO(n) (MESSy-field ECHAM and COSMO models nested n times) to localize the source area and to investigate the contribution from different source sectors. Section 4 finally summarises the findings of the present study.

2 Material and methods

2.1 Airborne instrumentation

Aircraft measurements were performed with the DLR Cessna 208B Grand Caravan within the scope of the Urban Climate Under Change program [UC]^2 (Scherer et al., 2019b). While the project's main objective is to develop, apply and validate an urban climate model at high spatial resolution (<10 m) for three German cities, our airborne observational wind and temperature data of Berlin were used for the validation subproject (Scherer et al., 2019a). One of our other objectives was to analyse the urban GHG emissions measured from the airborne platform. The aircraft was equipped with a series of instruments to measure meteorological parameters and trace gas species. The meteorological sensor package (METPOD) was mounted at the left underwing pod and included a boom with a five-hole probe at its tip for basic data like temperature (standard deviation σ = 0.15 K), pressure (σ = 0.25 hPa), humidity, wind direction (σ = 2°) and wind speed (σ = 0.3 m s^{-1}); for details see Mallaun et al. (2015). Wind measurements during strong turns (i.e. more than 10° roll

angle) were discarded for further analysis as deviations of up to 1 m s^{-1} are possible (personal communication with C. Mallaun, 2019). The AEROcontrol IGI system, which is a combination of differential GPS (Global Positioning System) and IRS (Inertial Reference System), provided aircraft position data. The following trace gas analysers were used with their backward facing inlets at the right underwing pod: (1) a Picarro cavity ring-down spectroscopy analyser (G1301-m) for CO_2, CH_4 and water vapour (H_2O); (2) a modified Aerodyne Quantum and inter-band Cascade Laser Spectrometer (QCLS) for CO_2, CH_4, ethane (C_2H_6), carbon monoxide (CO) and nitrous oxide (N_2O); for details see Kostinek et al. (2019); (3) a Cavity Attenuated Phase Shift (CAPS) Sensor for nitrogen dioxide (NO_2) and a 2B ozone (O_3) monitor.

For this study, we used CH_4 and CO_2 data at 0.5 Hz from the Picarro analyser (for a general description see Chen et al., 2010). During the campaign, the analyser was frequently calibrated on ground with four multi gas cylinders from Air Liquide. Before and after the deployment these secondary standards were calibrated against two NOAA (National Oceanic and Atmospheric Administration) multi gas primary standards (cylinder #CB11542 and #CB11361), which are traceable to the WMO-X2007 and WMO-X2004A scale (Dlugokencky, 2005; Zhao and Tans, 2006). The overall measurement uncertainty is determined to be better than 0.2 μmol mol^{-1} for CO_2 (hereafter referred to as ppm) and 1.1 nmol mol^{-1} for CH_4 (hereafter referred to as ppb) based on the summation of the known sources of uncertainty in quadrature, which are listed in **Table 1**. Details on the error estimate can be found in Sect. S1 in the supplement.

2.2 Aircraft-based mass balance approach

To infer CH_4 and CO_2 emission rates, the aircraft-based mass balance approach is a well-established method (e.g. Mays et al., 2009; Karion et al., 2013; Heimburger et al., 2017; Ren et al., 2018). A mass balance flight pattern typically includes one or multiple transects, that are in the ideal case aligned perpendicular to the wind direction and at an appropriate downwind distance from the source. Dependent on the study, they may also include an upwind transect to determine the background mixing ratios. The upwind transect usually is centred at the middle of the planetary boundary layer (PBL) and is used both to identify possible emission inflows (already being transported into the target region from a distant source) and to identify the natural atmospheric variability. The downwind transects, stacked at several altitudes within the PBL, capture the urban outflow downstream of the source. Vertical profiles, extending into the free troposphere, are used to determine the PBL depth. Flights are usually conducted in the afternoon, when the PBL is fully developed and its height is less variable during the time of the research experiment. Further assumptions are constant emission fluxes, steady wind speed and wind direction several hours before and during the flight experiment itself. The flux or mass flow rate [g s^{-1}] through a normal plane downwind of a source is then derived using Eq. (1):

$$f = \int_0^{PBL} \int_{-a}^{a} \left([c]_{ij} - [c_{bgr}]_{ij}\right) \frac{p_{ij}}{T_{ij} * R} M \;\; u_{ij} \; dxdz, \qquad (1)$$

The background mixing ratio c_{bgr} is subtracted from the observed mixing ratio c at location x_{ij} and z_{ij} and is converted to molar density using the ideal gas law with observed pressure p and temperature T, and the ideal gas constant R. Combined with the molar mass M and the perpendicular component u of the horizontal wind, a mass flow per unit area is obtained. By integrating along the horizontal boundaries of the plume ($-a$ to a) and in the vertical from ground to the top of the PBL, the mass flux through the plane is calculated. Uncertainties in the mass flux arise mainly from varying wind speed, the choice of background determination (e.g. using the mean or the lowest detected mixing ratios from an upwind transect or from edges of the downwind transects (Cambaliza et al., 2014; Peischl et al., 2015)), varying PBL depth, and limited observational data between the lowest altitude transect and the surface (Cambaliza et al., 2014).

Table 1: Estimated uncertainties for CO_2 and CH_4. For details see Sect. S1 in the supplement. DOI: https://doi.org/10.1525/elementa.411.t1

Sources of uncertainty	CO_2 [ppb]	CH_4 [ppb]
Precision	70	0.64
Water vapour	35.2	0.16
Drift with temperature	112.5	0.75
Drift with time	3.4	0.02
Reproducibility of primary standard	15.6	0.28
Reproducibility of secondary standard	44.8	0.33
Total uncertainty	145.1	1.09

2.3 Model setups

We use two different models to confine the source area and source origin related to our measurements. With the backward model HYSPLIT (Hybrid Single Particle Lagrangian Integrated Trajectory) we examine the source area of the encountered air masses. With the global/regional nested chemistry climate model MECO(n) we simulate the transport of emitted tracers based on different emission inventories to compare simulated GHG enhancements with airborne observations.

2.3.1 Lagrangian dispersion model HYSPLIT

A general description of the HYSPLIT model can be found e.g. in Stein et al. (2015). Here we use meteorological forecast data from the European Centre for Medium-Range Weather Forecasts (ECWMF) because of their high spatial and temporal resolution. Gridded fields are provided hourly with a horizontal resolution of 0.08° in latitude and 0.125° in longitude (~9 km × 9 km). The 137 model levels allow a vertical resolution of ~20 m near the ground, increasing to about 200 m at 3 km altitude.

We use backward trajectory calculations to reconstruct the pathway of the sampled air masses. Trajectories were started every 10 s from the flight track, while every 15 minutes along the trajectories information about latitude, longitude, height of the trajectory and depth of the model PBL are provided. These air histories can be used to define a so-called back trajectory (BT) footprint, which refers here to a more general definition of an area covered by the air mass within its residence time in the PBL. To do so, we first extract the BT points which were inside the PBL, and then determine their percentage residing in a defined grid box area between the downwind and upwind transects.

2.3.2 On-line coupled atmospheric chemistry model MECO(n)

The MECO(n) model couples on-line the global chemistry-climate model EMAC (ECHAM5/MESSy Atmospheric Chemistry) with the regional chemistry-climate model COSMO-CLM/MESSy in order to achieve a regional refinement (details can be found in Hofmann et al., 2012; Kerkweg and Jöckel, 2012a and 2012b; Mertens et al., 2016). COSMO-CLM (Rockel et al., 2008) is based on the COSMO (Consortium for Small scale Modelling) model and jointly further developed by the CLM-Community. For our campaign, a setup of three simultaneously running COSMO-CLM/MESSy instances nested into each other allows a fine horizontal resolution of 0.01° (~1 km × 1 km) over Berlin with 50 vertical model levels and a time step length of 20 s. In the global EMAC model (T42L90MA and 720 s) the prognostic variables temperature, divergence, vorticity and the logarithm of the surface pressure are nudged by Newtonian relaxation towards ECMWF operational analysis data. The COSMO-CLM/MESSy nests (i.e. over Europe at 0.44° and 240 s, over central Europe at 0.0625° and 60 s, and over NE Germany at 0.01° and 20 s) are directly driven by lateral and top boundary conditions from EMAC or from the corresponding coarser resolved nesting instance at each of the model time steps. The height of the midpoint of the uppermost grid box is approx. 80 km for EMAC and 22 km for COSMO-CLM/MESSy, respectively. A direct nudging of the COSMO-CLM/MESSy nests is not performed. Therefore, they can develop their own dynamics to a certain degree.

During the campaign, simulated wind fields and GHG mixing ratios were available from forecast simulations, and after the campaign from one corresponding analysis simulation. Mixing ratios of various GHG tracers have been simulated, where each individual tracer is subject to a specific emission source (or a set of emission sources) from different (individual or combined) inventories (see **Table 2**). Details about the inventories mentioned below are discussed in Sect. 2.4.

For the "city" tracer (c-CO_2, c-CH_4; see **Table 2**) we used an emission inventory provided by the city of Berlin (BERLIN inventory), that was gridded to a spatial resolution of 1 km × 1 km. This inventory provides detailed information about emissions from different sectors in Berlin as point, line and area sources and includes both air pollutants and GHG (AVISO GmbH and IE Leipzig, 2016). To account for surrounding emissions, we included strong point sources outside of Berlin, which were reported to the European Pollutant Release and Transfer Register (E-PRTR). For CO_2, eight facilities with combined emissions of 5.7 Mt CO_2 in 2016 were added (which is roughly $1/4^{th}$ to $1/3^{rd}$ of total Berlin emissions), for CH_4 this applies to two sources: landfill Schoeneicher Plan (south of Berlin) with 1.37 kt CH_4 in 2016 and landfill Neuenhagen (NE of Berlin) with 0.13 kt CH_4 in 2015. These simulated "city" tracers serve as baseline for the later analysis.

We further derived emissions for the "waste water" (w-CH_4) and "landfill" (l-CH_4) tracer according to Sect. 2.4.2, ranging from 1 to 7 kt CH_4 a^{-1} and from 0.1 to 32 kt CH_4 a^{-1}, respectively. To account not only for point sources outside of Berlin, but also the regional background, we merged the BERLIN inventory into the European CAMS-REG inventory (r-CO_2, r-CH_4). Since total CH_4 emissions for both inventories within Berlin differ by a factor of ~4.5 (see **Table 3**) it was necessary to scale the BERLIN CH_4 emissions with this factor to ensure that no artificial gradient in the simulated CH_4 mixing ratio is introduced at the boundary between the two merged inventories. For CO_2 no scaling was applied, however, grid boxes at the outermost boundary of BERLIN with very low emissions were removed.

During the model simulation the vertical profiles of all tracers (and several meteorological quantities) have been on-line sampled along the flight tracks (submodel S4D, described by Jöckel et al., 2010). This high-frequency output (at each model time step) is used for comparison

Table 2: Overview of the different tracers simulated with MECO(n) and the corresponding emission sources. DOI: https://doi.org/10.1525/elementa.411.t2

Tracer	Inventory input[a]
c-CO_2 ("city")	BERLIN + E-PRTR
c-CH_4 ("city")	BERLIN (×4.5) + E-PRTR
w-CH_4 ("waste water")	Status report of MLUL (2017) combined with EDGAR v4.3.2 waste water emissions from 2012
l-CH_4 ("landfills")	CORRECTIV (2016) as input for LandGEM
t-CH_4 ("total")	BERLIN × 4.5 + E-PRTR + w-CH_4 + l-CH_4
r-CO_2 ("regional")	BERLIN merged into CAMS-REG
r-CH_4 ("regional")	BERLIN (×4.5) merged into CAMS-REG

[a] For a detailed description of the inventories see Sect. 2.4, Figure 1 and Table 3.

Table 3: CO_2 and CH_4 annual emission fluxes (integrated within the Berlin city boundary in the upper two panels; corrected according to the footprint in the two lower panels) from the global EDGAR, European CAMS-REG and local BERLIN inventory. DOI: https://doi.org/10.1525/elementa.411.t3

	EDGAR 2015	CAMS-REG 2015	BERLIN 2012	EDGAR 2015	CAMS-REG 2015	BERLIN 2012
Emission sector	CO_2 [Mt a^{-1}][a]			CO_2 [%][a]		
Total	24.2	22.6	16.8	100	100	100
(ff + bf)	(22.5 + 1.7)	(15.4 + 7.1)				
Fuel combustion for the generation of electricity and heat	19	17.9	13.7[e]	79[b]	79[c]	82[e]
	(17.5 + 1.5)[b]	(12.5 + 5.4)[c]				
Road transport	2.4	2.5	2.7[f]	10	11	16[f]
	(2.3 + 0.1)	(2.4 + 0.1)				
Others	2.8	2.2	0.4	12	10	2
	(2.7 + 0.1)	(0.5 + 1.6)				
Emission sector	CH_4 [kt a^{-1}]			CH_4 [%]		
Total	25.7	15.4	3.4	100	100	100
Waste	20.3[d]	0.1	0.1	79[d]	1	3
Fuel combustion for the generation of electricity and heat	2[b]	5.6[c]	0.8[e]	8[b]	36[c]	24[e]
Fuel exploitation	2.6	5.8	2.3	10	38	68
Others	0.8	3.9	0.2	3	25	5
Footprint corrected total[g]	CO_2 [Mt a^{-1}]			n.a.		
	41.9	30.6	n.a.			
Footprint corrected total[g]	CH_4 [kt a^{-1}]			n.a.		
	94.3	21.9	n.a.			

[a]The first column lists the emission fluxes for different emission sectors in Mt or kt per year [a^{-1}], the second column shows the relative share in percent. CO_2 is split into contributions from fossil fuel and biofuel when possible and indicated by parentheses (ff + bf).

[b–f]The EDGAR sector definitions follow the IPCC 1996 code, while CAMS-REG and BERLIN are sectored according to the SNAP (Selected Nomenclature for Air Pollution) categories.

[b]Sum of sector energy for buildings, combustion for manufacturing, and power industry.

[c]Sum of sector SNAP 1 (combustion in energy and transformation industries), SNAP 2 (non-industrial combustion plants) and SNAP 34 (emissions which cannot be clearly attributed to SNAP 3 (combustion in manufacturing industry) or SNAP 4 (production processes)).

[d]Sum of sector solid waste incineration, solid waste landfills, and waste water treatment.

[e]Sum of SNAP 1, SNAP 2, SNAP 3, SNAP 4, SNAP 34, and extra category of heating.

[f]Sum of minor roads and major roads. Emissions for minor roads were estimated based on NO_x emissions from the same inventory using the constant emission ratio for major roads (CO_2/NOx factor of 355.5 ± 45.4 kg CO_2/kg NOx; see Kuhlmann et al., 2019a). Emissions for major roads were compiled from earlier inventories. Therefore, road transport emissions might slightly differ from Berlins official numbers.

[g]The footprint corrected total emissions for CO_2 and CH_4 are given for the EDGAR and CAMS-REG inventory (for details see Figure 7 and corresponding text).

with the observations. We refrain from computing simulations with the EDGAR emissions, as the inventory is a factor ~10 coarser than the MECO(n) model resolution (~1 km × 1 km). Hence, using such a coarse emission inventory with a much finer model resolution will not add useful information.

2.4 Greenhouse gas emission inventories

2.4.1 Inventorial emissions

In this section we compare three available GHG emission inventories from global to local scales for the city of Berlin and its surrounding area: (a) the global inventory EDGAR v5.0 for the year 2015 with a resolution of 0.1° × 0.1° (Crippa et al., 2019); (b) the European inventory CAMS-REG v1.1 for 2015 with a resolution of 0.0625° × 0.125° (Kuenen et al., 2014); and (c) a local Berlin inventory, referred to as BERLIN, for 2012 (Berliner Emissionskataster v1.0, AVISO GmbH and IE Leipzig, 2016), provided by the Senatsverwaltung für Stadtentwicklung und Umwelt Berlin (A. Kerschbaumer). The latter inventory consists of individual area, point and line sources which for this study have been projected to a 0.01° × 0.01° longitude-latitude grid (~1 km resolution). Parts of this inventory are described by Brunner et al. (2019) and by Kuhlmann et al. (2019a).

Figure 1 shows the CO_2 (upper row) and CH_4 (lower row) emission maps for the EDGAR (panels a), CAMS-REG (panels b) and BERLIN (panels c) inventories, respectively, along with the city boundary of Berlin. **Table 3** lists the estimated CO_2 and CH_4 emission totals within the city boundary together with the main contributing sectors in detail. The first column presents for each inventory the emissions in Mt CO_2 and kt CH_4 per year [a^{-1}], while the second column lists the relative share of the sectors in percent. CO_2 is split into contributions from fossil fuel (ff) and biofuel (bf) for the EDGAR and CAMS-REG inventory (see parentheses in **Table 3**), while for the BERLIN inventory this information is not available. Total CO_2 emissions from Berlin range from 16.8 to 24.2 Mt a^{-1} between different inventories and thus agree within a factor of ~1.4. The CO_2 emissions (note that all CO_2 maps are plotted in the same colour range in **Figure 1**) are rather confined to the inner city, since they are closely coupled to fossil fuel consumption related to energy production and transport (Helfter et al., 2011), and thus to areas with high population density and locations of power plants. This is also reflected in the emission sectors, as the majority of emissions (79 to 82%) within the three inventories are related to fuel combustion for the generation of electricity and heat. The emission strength itself, however, is different, while the inventories agree in the numbers for the road transport sector. According to EDGAR, the relative CO_2 contribution from the road traffic sector for Berlin (~10%) is slightly lower than for greater Paris (~16%) or London (~22%). This is most likely explainable by the high dominance of point source emissions from power plants located within the city of Berlin. Roughly 94% of point source CO_2 emissions reported to E-PRTR in 2016 was released from power plants. In contrast, these emissions only account for zero and ~21% for the inner and outer city of London, respectively, and for ~24% for Paris. Strong CO_2 sources outside the city are located at different spots when comparing EDGAR and CAMS-REG.

With respect to CH_4, larger discrepancies are present between the inventories; both in the partitioning into different sectors and in the magnitude of emissions (factor ~8). Therefore, each CH_4 panel has its own colour scale. In EDGAR, strongest CH_4 sources are located outside the city and mainly consist of solid waste landfills and waste water handling. In contrast, emissions reported in CAMS-REG are mainly due to fuel combustion for the generation of electricity and heat and fuel exploitation, with only little contribution of waste treatment and disposal. Hence, the spatial distribution of CH_4 emissions is similar to the CAMS-REG CO_2 emission distribution. Interestingly, BERLIN also reports almost no emissions from the waste sector, the main contribution of 2.3 kt CH_4 a^{-1} results from leakages during natural gas transport in pipelines and during storage in gasometers. According to the report for the Berliner Emissionskataster (AVISO GmbH and IE Leipzig,

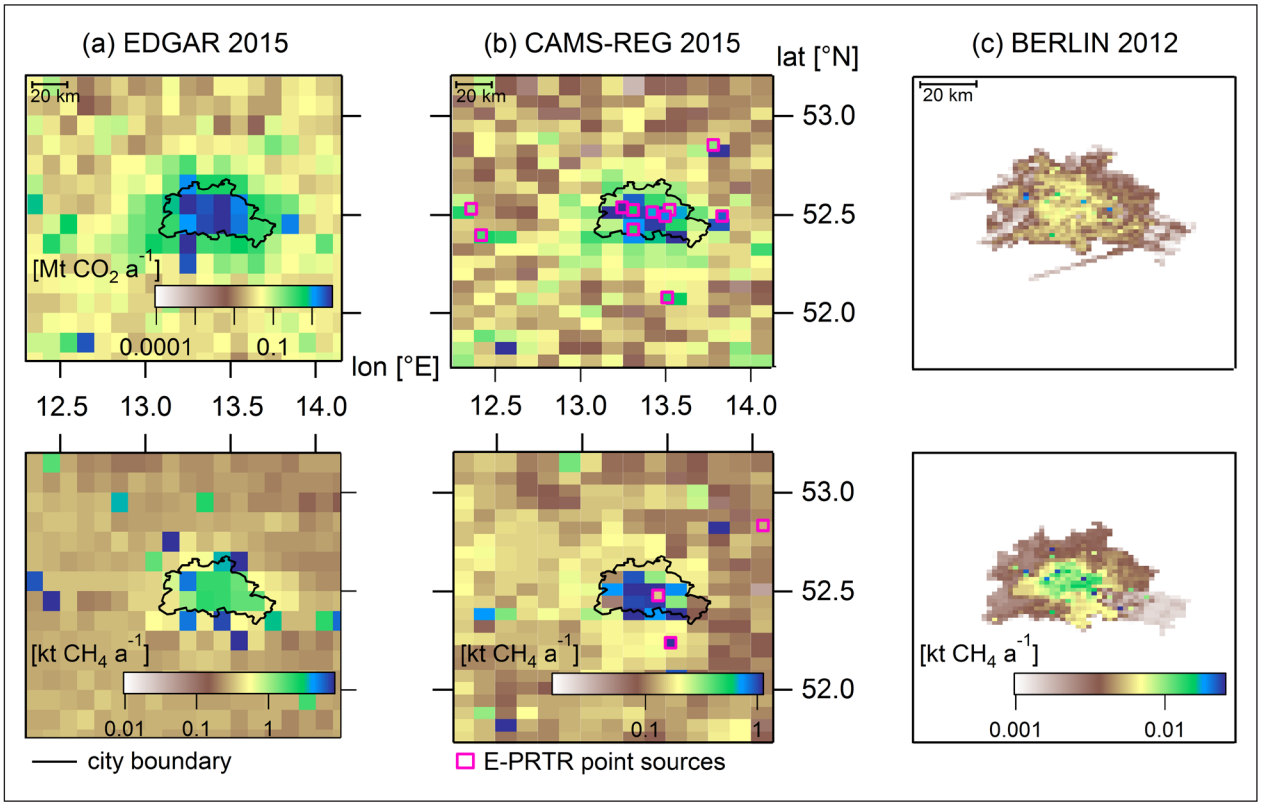

Figure 1: Emission maps for the Berlin area. Emission maps are shown for CO_2 (upper row; same colour scale for every panel) and CH_4 (lower row; different colour scales) from three inventories: **(a)** EDGAR v5.0 for 2015 with a resolution of 0.1° × 0.1°; **(b)** CAMS-REG for 2015 with a resolution of 0.0625° × 0.125°, superimposed are selected point sources from E-PRTR for simulation purpose (see Sect. 2.3.2); **(c)** BERLIN inventory for 2012 with a resolution of 0.01° × 0.01°. The horizontal stripes in CO_2 are due to take-off and landing at the two major airports. Note that the BERLIN inventory is slightly enlarged (distance scale). DOI: https://doi.org/10.1525/elementa.411.f1

2016), waste treatment in municipal sewage-treatment facilities occurs under aerobic conditions (where no CH_4 is produced) and composting facilities of organic waste (where CH_4 can be produced) are located outside of Berlin and are thus neglected in the inventory. In contrast, EDGAR uses for solid waste disposal and waste water emissions a proxy mainly based on the distribution of urban and rural population (Janssens-Maenhout et al., 2012).

For **Table 3** we estimated the emissions in EDGAR and CAMS-REG based on the percentage of the grid cell area being within the city boundary based on OpenStreetMap (2018), which uses an administrative boundary dividing Germany into 16 federal states, including Berlin. The population is less dense in the surrounding state Brandenburg (with 84 inhabitants per km^2) compared to Berlin (4055 inhabitants per km^2; Strukturatlas Land Brandenburg, 2017). For details see Figure S9 in the supplement. A sensitivity test, where only the grid cells in EDGAR (CAMS-REG) were taken, which contain at least 75% of the city area, reveal that total emission estimates are lower, both for CH_4 with ~25% (20%) and for CO_2 with ~7% (4%). Nevertheless, the large discrepancies between the CH_4 inventories cannot be explained by this, as total CH_4 emissions still vary by a factor of ~6.

Member states of the EU further have to report emissions from single industrial facilities to the European Pollutant and Transfer Register (E-PRTR), if their release to air exceeds a threshold of 0.1 Mt a^{-1} for CO_2 or 0.1 kt a^{-1} for CH_4 (http://prtr.ec.europa.eu/#/pollutantinfo, last access: 18.09.2019). In **Figure 1b** these point sources are superimposed on the CAMS-REG inventory to point out that locations of hot spots (and their source strengths) do not always match between EDGAR and CAMS-REG, and thus to highlight the importance of an experimental verification of GHG emissions around Berlin.

2.4.2 Additional CH_4 emissions from waste water treatment plants and illegal landfills

As described above, CH_4 emissions show large discrepancies between the three different inventories, especially with respect to the waste sector. Therefore, we collected additional information on locations of sewage-treatment plants and on unofficial waste deposits, which reflect strong point sources. We derive corresponding CH_4 emissions and implement them as separate tracers in the MECO(n) model simulation (see **Table 2**) to determine their source strengths individually, and to compare them to the other emissions.

Figure 2a shows sewage-treatment facilities superimposed on the EDGAR v5.0 waste water CH_4 emission map from 2015. We took information on sewage-treatment plants from a status report of the Ministerium fuer Laendliche Entwicklung, Umwelt und Landwirtschaft (MLUL, 2017) and determined their exact position with Google Earth. Since the report only covers the state of Brandenburg, we added the one sewage-treatment plant within the Berlin city boundary (Ruhleben, Berliner Wasserbetriebe). As obvious in **Figure 2a**, larger plants surrounding Berlin (they are sized according to their population equivalent) correlate very well with pixels of stronger EDGAR CH_4 emissions. Therefore we transferred their emissions and assigned the remaining smaller facilities with an arbitrarily chosen CH_4 rate of 1 kt a^{-1} to ensure a visible signal in the model output (note that although

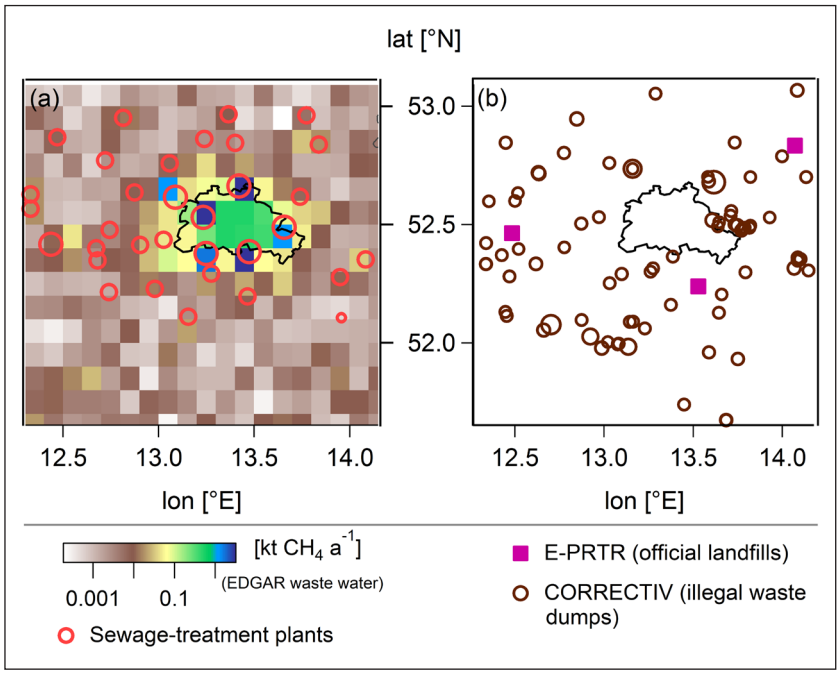

Figure 2: CH_4 emissions from sewage-treatment plants and illegal landfills. (a) Sewage-treatment plants (MLUL, 2017) are sized according to their population equivalent and superimposed on the EDGAR v5.0 waste water CH_4 emission map. **(b)** Illegal waste deposits (CORRECTIV, 2016) are sized according to the amount of deposited waste (ranging from 0.06 to 416 kt of waste). Official landfills listed in E-PRTR are not sized. DOI: https://doi.org/10.1525/elementa.411.f2

Figure 2a shows the EDGAR v5.0 waste water map of 2015, the values from 2012 (v4.3.2) were assigned to the facilities as the model run was not repeated after updating to the most recent inventory v5.0). Landfills are another well-known CH_4 emission source, which we consider separately. In **Figure 2b** official landfills (reported by E-PRTR) are mapped together with illegal waste dumps, which are based on information from the non-profit organization *CORRECTIV*. Their article reveals that more than 100 illegal landfills in Brandenburg contain at least three million tons of waste; however, the legal disposal would cost more than 320 million Euros (CORRECTIV, 2016). We calculated CH_4 emissions using the Landfill Gas Emission Model (LandGEM, 2005, v3.02), provided by the United States Environmental Protection Agency (EPA). Input parameters are the amount of waste and the year of the first deposit as waste is continuously decomposing. If no information on the year was available, we used the most frequently reported (i.e. year 2000). Furthermore, we assumed a constant decay rate ($k = 0.038$) and a degradable organic carbon content ($DOC = 0.2028$) based on moderate climate, and assuming all waste material being from municipal solid waste landfills (EPA, 2010). Estimated CH_4 emissions range from 0.002 to 16 kt a^{-1}. We do not claim that calculated emissions from sewage treatment and landfills represent true values, however, they serve as input for model sensitivity tests to study the importance of these sectors (see Sect. 3.3.1).

3 Results and discussion

3.1 Flight strategy and mission overview

As discussed in Sect. 2.2 we optimised the mission flight strategy to study GHG fluxes of Berlin using the mass balance approach. Our flight planning mainly relied on the MECO(n) plume forecast of the GHG city tracers c-CO_2 and c-CH_4 (see **Table 2**). With horizontal latitude-longitude projections as well as vertical height profiles, we determined the location of the urban pollution plume and the distance at which the plume is supposed to be vertically well mixed. Furthermore, we used the meteogram for Berlin-Tempelhof provided by the German Weather Service (Deutscher Wetterdienst, DWD) on the basis of their ICON (Icosahedral Nonhydrostatic) forecast model, as well as animated forecasts based on ECMWF and GFS (Global Forecast System) from *windy.com* to verify the wind forecasts from MECO(n). Flight plans had to be submitted to air traffic control (ATC) on the day before the flight and were approved (either as submitted or slightly modified) shortly before the flight. However, discrepancies between the previous day forecast and the actual wind conditions, together with the heavy air traffic situation in and around Berlin with its two major airports (Berlin-Tegel and Berlin-Schoenefeld), generally hampered the realization of the flight patterns, which were designed for optimized sampling of the in- and outflow.

Five research flights were conducted with the DLR Cessna aircraft between 16th and 26th of July 2018 from the airfield Schoenhagen, located ~40 km southwest of Berlin (see **Figure 3**). The typical mass balance pattern was roughly perpendicular to the prevailing wind direction, which was mainly from NW to NE. Flights were conducted between ~11:30 and ~15:00 UTC (+2 hours for local time) to ensure a fully developed PBL. To characterise the PBL during each flight, we obtained a vertical profile (upward spiral, typically between 0.3 and 3 km) at the Tempelhofer Feld (TF, south of the city centre). The horizontal extent of Berlin is approximately 35 to 45 km. In order to assure complete sampling of the urban outflow, the length of our

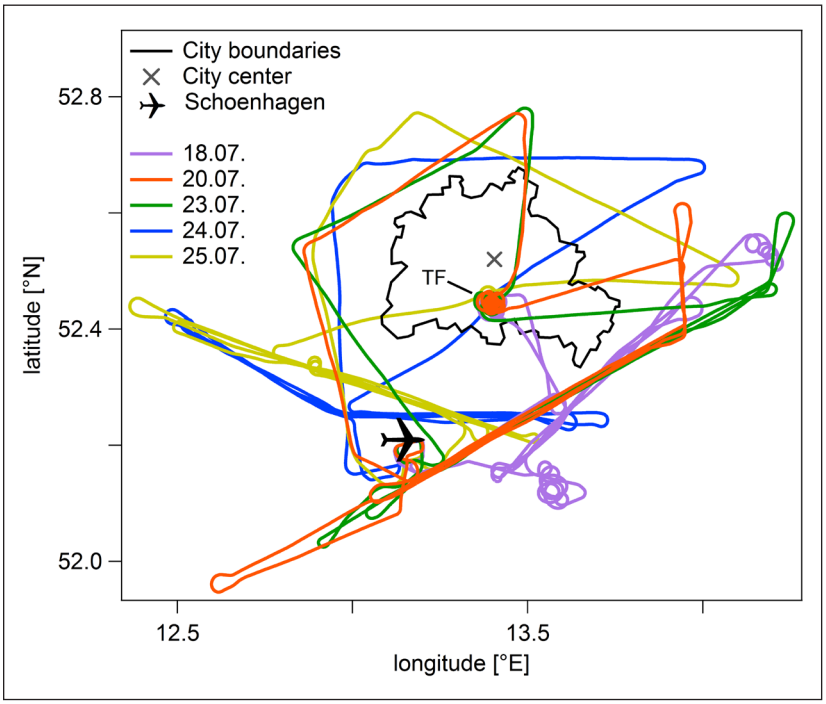

Figure 3: Flight paths of the DLR Cessna. At the Tempelhofer Feld (TF), located south of the city centre, an upward spiral was flown during each flight to characterise the boundary layer. DOI: https://doi.org/10.1525/elementa.411.f3

stacked downwind transects (so-called "wall") was planned to cover more than 80 km distance at a typical downwind distance of roughly 30 to 40 km. **Table 4** presents an overview of all research flights including date, flight time, average wind direction, average wind speed, PBL depth (estimated from the meteorological measurements, see Sect. S2) and the general weather situation. Time series for CO_2, CH_4 and flight altitude of each flight can be found in Figure S1, as well as altitude profiles of virtual potential temperature, static temperature, and relative humidity to estimate the PBL depth in Figure S2.

In the following section we apply and discuss the mass balance approach for the case study on July 20th as strong CO_2 and CH_4 signals from urban emissions were distinguishable from the atmospheric background variability together with ideal meteorological conditions prevalent on that day. For the flight on July 24th the limitations of the mass balance approach are discussed in Sect. 3.3.2. We further excluded the remaining three performed flights (on 18th, 23rd and 25th of July) from the mass balance analysis due to the following reasons: Based on **Table 4** and Figure S2 it is apparent that the PBL on July 18th and 25th is not clearly separated from the free troposphere and not well-mixed. In addition, the wind speed on July 18th is rather high with more than 8 m s^{-1} on average. On July 23rd meteorological conditions appeared to be favourable, however, the urban plume is most likely missed, mainly because of the large difference between forecasted and real wind direction (~40°) and the inflexibility to adapt the submitted flight pattern ad hoc due to air traffic control restrictions.

3.2 Mass balance flight on July 20th

3.2.1 Flight pattern and airborne observations

On July 20th the research flight was conducted between ~11:30 and ~14:00 UTC. The flight pattern is shown in **Figure 4a**, the time series of the measured mixing ratios

Table 4: Overview of five performed research flights. DOI: https://doi.org/10.1525/elementa.411.t4

Day of July 2018 (weekday)	Take-off and landing [UTC]	Avg.[a] wind direction [deg]	Avg.[a] wind speed [m s^{-1}]	PBL depth[b] [m]	Weather situation
18th (Wed.)	11:35–14:13	304 ± 14	8.5 ± 1.8	1079 ± 26 2648 ± 7[c]	West of occlusion along border Germany/Poland
20th (Fri.)	11:30–14:07	299 ± 27	4.8 ± 1.8	2737 ± 2	Ridge of high pressure system, low level clouds
23rd (Mon.)	11:37–14:08	296 ± 16	5.6 ± 1.4	1419 ± 4	Clear sky
24th (Tues.)	12:12–14:59	25 ± 34	3.3 ± 1.3	2046 ± 1	Eastern edge of high pressure system, low level clouds
25th (Wed.)	11:28–14:10	27 ± 28	3.3 ± 1.1	1969 ± 56	South-eastern edge of high pressure system, low level clouds

[a] For the average wind speed and direction the average of the whole flight is considered, excluding winds above the PBL when different.
[b] PBL depth is estimated from meteorological measurements, see Sect. S2.
[c] PBL has two layers.

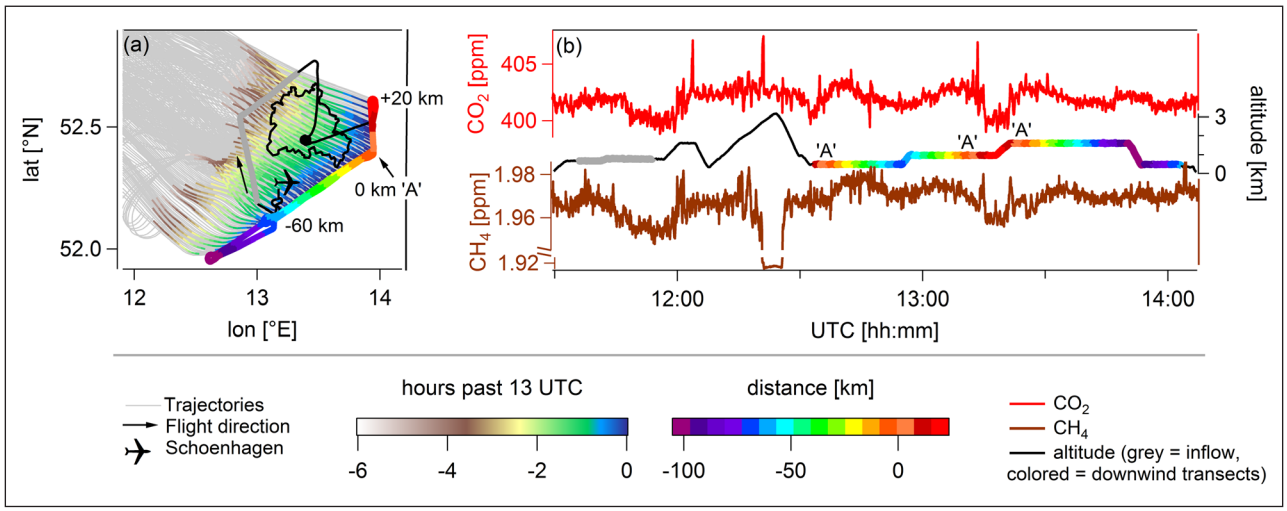

Figure 4: Flight pattern and time series of July 20th. (a) The downwind wall is colour-coded according to the flown horizontal distance (0 km corresponds to the starting point 'A' at 52.41°N and 13.95°E). Backward trajectories (−12 h, in grey) are started from the downwind "wall" at 13 UTC, while every 5th trajectory within the PBL is colour-coded according to its relative time since the calculation start. **(b)** The grey sections of the altitude curve correspond to the inflow section of the flight; other colours same as in panel (a). DOI: https://doi.org/10.1525/elementa.411.f4

of CO_2 and CH_4, as well as flight altitude are presented in **Figure 4b**.

Forecasts indicated north-northwesterly winds and a boundary layer height of ~2 km. However, during the flight itself, the wind came from the north-west with 4.8 m s^{-1} on average. We first headed towards the north (indicated by the black arrow in **Figure 4a**) to perform the upwind leg roughly at the middle of the PBL (~780 m). This upwind section is shaded grey on the altitude curve visible in **Figure 4b**. A detailed vertical profile was obtained at the Tempelhofer Feld from ~350 m up to ~3.2 km (with an ascend rate of ~3 m s^{-1}), hereby detecting the lowest CH_4 mixing ratios during the entire flight (note the split CH_4 axis; see also vertical profile in **Figure 5c**). The in-flight derived PBL height from the vertical profile was then used to adapt the heights of the following downwind transects to roughly 500 m, 1 km and 1.6 km. This so-called downwind "wall" is colour-coded in both panels according to the horizontal flown distance. Sampling of the urban plume started at point 'A' (marked with 0 km distance) towards the south-west (indicated with negative distances). Since in-flight observations of atmospheric GHG mixing ratios did not reach background concentration levels as observed at the starting point, we extended the downwind transects in-flight. Due to air space restrictions this was only possible by flying strictly towards the north (indicated with positive distances). **Figure 4a** also includes HYSPLIT backward trajectories for the last 12 hours, which were started from the entire downwind "wall" at 13 UTC. Colour-coded is (for simplicity) only every 5th trajectory within the PBL to its relative time since its calculation start. The grey colours underneath depict, in addition, also trajectories being outside the PBL. The trajectories reflect the prevalent wind direction and wind speed quite well (ECMWF forecast data and airborne wind measurements reveal Pearson correlation coefficients between R = 0.95 and R = 0.98; for details see Figure S4 and S5) and indicate a steady wind flow within the PBL for at least 6 hours prior to our measurement.

Figure 5a presents the measured CO_2 (upper panel) and CH_4 (lower panel) mixing ratios along the horizontal distance at the three different altitudes of our "wall". The encountered CO_2 plume is detected approximately between −30 and 15 km, thus in the more northern part of our flight track, whereas the centre of the CH_4 plume extends more to the south-west (roughly between −50 and 15 km). A similar CO_2 distribution was observed at all altitudes with maximum enhancements of 4 ppm, indicating a generally well-mixed plume. Measured CH_4 mixing ratios in the two lower flight levels are also coherent with enhancements of 21 ppb, but the highest flight level shows a different pattern with a dip in CH_4 between −20 and 0 km. Differences in the vertical distribution of CO_2 and CH_4 can be explained by a combination of three effects: a) differences in the

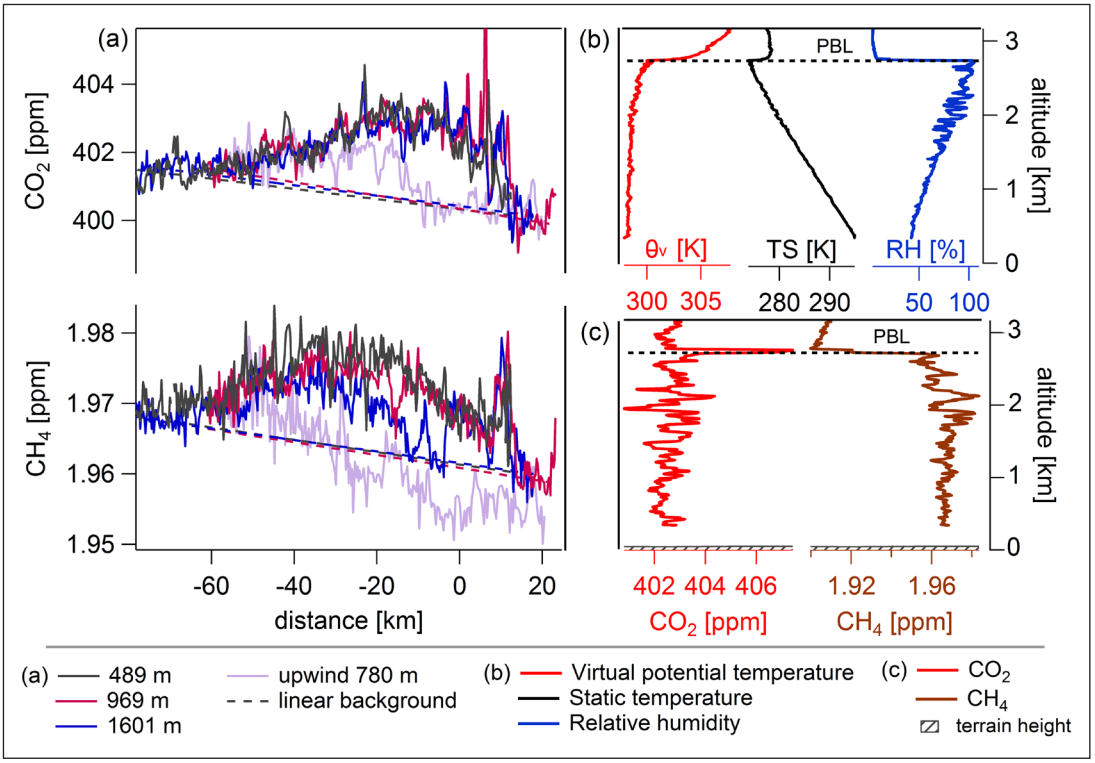

Figure 5: Downwind GHG mixing ratios and vertical profile at the Tempelhofer Feld of July 20th. (a) Measured CO_2 and CH_4 mixing ratios (segment mean) at three different altitudes within the PBL along the flown horizontal distance. The background based on the edges of the flight leg is shown with dashed lines, the background based on mixing ratios measured upwind as light purple line (see Sect. 3.2.2 for details). **(b)** Vertical profile of virtual potential temperature (θ_v), static temperature (TS) and relative humidity (RH) at the Tempelhofer Feld. The derived PBL depth is shown as black dashed line. **(c)** Vertical profile of CO_2 and CH_4 at the Tempelhofer Feld, the terrain height of ~43 to ~50 m reflects the west to east cross-section at the Tempelhofer Feld retrieved from Google Earth. DOI: https://doi.org/10.1525/elementa.411.f5

spatial distribution of the emissions sources (see Sect. 2.4), b) differences in the emission height, and c) differences in the buoyancy of the gases at their release point. CO_2 is largely emitted via stacks, already occurring at a certain elevated height above ground level, which may influence the distribution due to the altitude dependent wind speed and direction (Brunner et al., 2019). Furthermore, CO_2 emissions are closely coupled to fossil fuel consumption and thus to higher temperatures during the release, which enhance the buoyancy of the air parcels and the mixing in the vertical. In contrast, CH_4 emissions are usually not emitted during exothermic processes, therefore the vertical mixing might be less pronounced. In addition to these broad enhancements, some small-scale enhancements (~3 to 5 km wide peaks) are observed at ~7 km distance (in CO_2) and further north at ~11 km (in CH_4).

Figure 5b shows the vertical profile obtained at the Tempelhofer Feld (from roughly 12:00 to 12:30 UTC) of virtual potential temperature (θ_v), static temperature (TS) and relative humidity (RH). The PBL depth was determined from that profile to 2737 ± 2 m (dashed black line), where the uncertainty of 2 m reflects the average of the three different approaches used herein (see Sect. S2 in the supplement). The PBL on July 20th was well-mixed and efficiently capped as seen in the strong gradients in θ_v, TS and RH between the PBL and the free troposphere. The PBL depth also agrees well with aerosol lidar measurements at Leipzig performed within the European Aerosol Research Lidar Network (EARLINET), indicating a PBL depth of roughly 2600 m at 14 UTC (see Figure S3).

3.2.2 Greenhouse gas flux results

Our measurements on July 20th, presented in **Figure 5a**, show that the urban CO_2 plume is well-mixed at the different sampling altitudes between ~500 m and ~1600 m, which is also well represented by the MECO(n) model (see **Figure 8c** later). The vertical mixing of the CH_4 plume seems slightly less pronounced, as indicated by the measurements of the highest altitude transect (see **Figure 5a** and previous Sect. 3.2.1). Based on the simulated vertical GHG distribution within the entire PBL at the downwind transects (see Figure S10 and Sect. S8 in the supplement for further details), we further deduce that the CO_2 emissions are also well-mixed above and below our flight altitudes and more specifically, throughout the PBL, where emissions are efficiently trapped by the strong inversions (as illustrated by the meteorological measurements in **Figure 5b**). We then estimate the emission rate individually for each single transect, similar to the method described by e.g. Karion et al. (2013) and Peischl et al. (2013). Thereby, actual wind (and temperature and pressure) measurements are considered at each single GHG measurement point. The estimated mass flux then is derived as the mean from the three single mass fluxes, which also account for the less homogeneous distribution of the CH_4 plume. As introduced in Sect. 2.2 and shown in Eq. (1), uncertainties in the mass flux are influenced by uncertainties in the choice of background determination, wind speed, wind direction and varying PBL depth. **Table 5** lists the emission rate estimate and sources of uncertainties, which are discussed in the following.

We illustrate two approaches to obtain the atmospheric background mixing ratio (see **Figure 5a**). The first approach uses the linear interpolation of atmospheric mixing ratios between the plume edges (indicated by the dashed lines). For this, the plume was defined as when the measured mixing ratios exceeded the inward running mean (interval of ±30 s) plus one standard deviation (only for CO_2) for at least five consecutive measurement points. The atmospheric background is then calculated using the average of 60 measurement points outside the plume. One exception is the south-western end of the intermediate CH_4 transect (i.e. at negative distances), which is marked in purple. Due to missing observational data in that transect, we did not observe a decrease in CH_4 mixing ratios down to lower (and hence, atmospheric background) values as detected for the other two transects (indicated in grey and blue). In this case, we therefore used the mean CH_4 background determined from the other two transects. Each altitude transect thereby is treated separately to account for possible vertical atmospheric gradients, and both sides of each transect are considered to capture the horizontal gradients.

In a second approach to obtain the atmospheric background, the mixing ratios measured during the upwind leg (indicated by the light purple line in **Figure 5a**) were projected on the downwind wall using the calculated HYSPLIT trajectories. It is assumed that the mixing ratios from the upwind leg are valid for the entire PBL (i.e. for all three transects). Using that approach, we still obtain quite good agreement between the CO_2 mixing ratios measured on both edges of the downwind plume and in the upwind leg. However, the measured CO_2 mixing ratios in the inflow leg are somewhat larger than the linearly interpolated background. For CH_4, the slope of the SW to NE gradient is steeper in the inflow leg compared to the slope in the downwind observations. The large impact of the choice of background is reflected in the resulting flux calculations, which differ by nearly 50% in the case of CO_2. Using the first approach, we obtain a stronger flux (2.12 t CO_2 s^{-1}) compared to the second approach (1.39 t CO_2 s^{-1}). For CH_4, the mean fluxes do not differ as much (21%). It is worth noting that the upwind leg was flown between ~11:35 and ~12:00 UTC, while the downwind wall was probed between ~12:30 and ~13:50 UTC. Consequently, with an average measured wind speed of 4.8 m s^{-1} and a distance of ~50 km between the up- and downwind

Table 5: Estimated mass flux and uncertainties for CO_2 and CH_4 for July 20th. DOI: https://doi.org/10.1525/elementa.411.t5

	CO_2	CH_4
Mass flux	[t s^{-1}]	[kg s^{-1}]
	1.39 ± 0.76	5.20 ± 1.70
Uncertainties	[%]	[%]
Choice of background	±52	±21
Wind speed and direction	±15	±23
PBL depth variation	±9	±10

transects, the air was not sampled in a Lagrangian manner. Such sampling involves first the measurement of an air mass at a specific starting location, and second the re-sampling of the same air mass after it has been transported to a new location. These observations demonstrate the importance of separating the urban plume from enhancements caused by emissions from anthropogenic sources (or natural variability) upstream of the city, even in the case of an apparently relatively isolated city as Berlin (see population density in Figure S9). Upwind of the flight track (to the east and west) two large nature parks are located (Naturpark Westhavelland, Biosphärenreservat Schorfheide-Chorin) with two municipalities in between (Neuruppin and Zehdenik) having a population density of only 50 to 100 inhabitants per km^2 (see also Figure S9). With respect to **Figure 1**, their location is still included in the plots (at ~53°N and 12.8°E; ~53°N and 13.3°E, respectively), however, neither EDGAR nor CAMS-REG indicate any relevant sources of CO_2. For CH_4 (at least in EDGAR) two grid cells in the vicinity are coloured in green, indicating emissions from solid waste disposal.

Similar to Cambaliza et al. (2014), we calculated the influence of the uncertainty of the wind on the estimated flux by $\Delta flux/\Delta u$ with $\Delta flux$ being the change in the flux and Δu being the uncertainty in the perpendicular wind component. The measurement uncertainties in wind direction (±2°) and wind speed (±0.3 m s^{-1}) translate into errors of ±15% in the CO_2 flux and ±23% in the CH_4 flux. On July 20th we only penetrated the free troposphere once, but comparable conditions (i.e. pronounced inversions) were also prominent on July 18th (see Figure S2). On July 18th we performed two vertical profiles separated by approximately two hours and observed only a difference of ~50 m (~2%) in the PBL depth. If we assume that no significant PBL variation (<2%) occurred during the flight on July 20th, the errors are small in the estimated fluxes (<1%). To test the sensitivity of the derived mass fluxes on the PBL depth variability, we calculated the errors for larger variations as well. In the case the PBL depth would change by 5 to 10% (roughly 140 to 270 m), the errors in the estimated fluxes (<10% for the CH_4 flux and <9% for the CO_2 flux) are still smaller than the uncertainty arising from wind speed and wind direction (15% for CO_2 and 23% for CH_4, see **Table 5**). Entrainment and detrainment from the free troposphere, another possible source of error, can be excluded in this case due to the pronounced inversions at the top of the PBL (see **Figure 5b**). Considering all sources of uncertainties, our emission estimate (our emission estimate results in) results in 1.39 ± 0.76 t CO_2 s^{-1} and 5.20 ± 1.70 kg CH_4 s^{-1} (see **Table 5**). For this calculation the second approach to obtain the atmospheric background was chosen, hence, important information of the inflow are considered, which obviously should not be neglected in the case of Berlin. However, we also included the first approach (using the edges of the downwind track) as uncertainty estimate, since the use of the up- and downwind transects has the disadvantage, that the air masses were not sampled in a Lagrangian manner.

3.2.3 Discussion on emission fluxes

To be able to compare our flux estimate with the corresponding area of the three emission inventories EDGAR, CAMS-REG and BERLIN (see Sect. 2.4), we first determine a footprint area with HYSPLIT. The footprint reflects the percentage of the air mass within the PBL at a specific location (of a defined latitude-longitude grid) between the upwind and the downwind track (see Sect. 2.3.1). To determine the horizontal edges, backward trajectories were released only for GHG enhancements greater than zero after subtracting the upwind mixing ratios from the observed downwind mixing ratios.

Figure 6 gives the flight path of July 20th, where the downwind wall is colour-coded according to the GHG enhancement, and the footprint analysis is shaded with

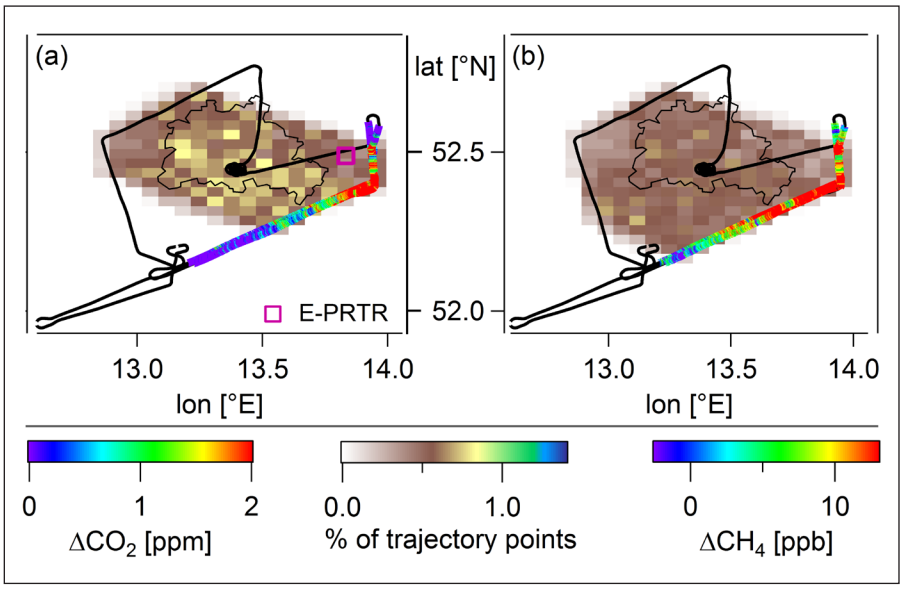

Figure 6: CO_2 and CH_4 footprint of July 20th. Footprint corresponding to a grid box of 0.03° × 0.065° for **(a)** the CO_2 and **(b)** the CH_4 plume detected on July 20th. The purple marker in panel (a) indicates the location of three point sources from E-PRTR, which are located within a 1 km radius next to each other. DOI: https://doi.org/10.1525/elementa.411.f6

respect to the observed CO_2 and CH_4 plume. The distribution of trajectory points in **Figure 6a** is relatively homogeneous and indicates that the CO_2 plume covers the entire city. The sharp spikes in CO_2 (see **Figure 5a** at roughly 7 km distance) are detected directly downwind of three CO_2 point sources listed in E-PRTR: Fels-Werke GmbH, CEMEX Zement GmbH, and Vattenfall Europe New Energy Ecopower GmbH. They are located within a 1 km radius next to each other (marked in orange) and together report emissions of 1.9 Mt CO_2 in 2016. In contrast, the footprint of the CH_4 plume (**Figure 6b**) indicates that sources in the south-west outside of Berlin contribute to the measured CH_4 enhancement.

In a next step, we scale our flux estimate to a yearly value (regardless of diurnal, weekly or seasonal cycles), the result is shown in **Figure 7** with blue bars. Grey bars denote emissions of CAMS-REG, EDGAR and BERLIN within the Berlin city boundary. The striped bars represent emissions from the footprint-corrected inventories of CAMS-REG and EDGAR, i.e. the emissions in the inventory grid cells, which are covered by the footprint area, are added up. Thus, we get 35 to 75% larger emission rates for CO_2 and 40 to 270% larger emission rates for CH_4 if we consider the sources which are located outside the definition of the city boundaries. According to Stohl (1998), trajectories may deviate by 10% of their travelled distance. Thus, the footprint area for this case study might be mislocated by up to ~7.5 km. The resulting deviation in the total inventorial emissions is considered by the error bars in **Figure 7**.

For the flight on July 20th, our annual CO_2 emission rate of ~44 ± 24 Mt a^{-1} is larger than the CAMS-REG and the EDGAR footprint estimates, but agrees within the error bars. Previous studies showed, that urban CO_2 emissions based on EDGAR (especially related to the road transport sector) are likely overestimated, however these studies only focused on American cities (e.g. Gately et al., 2013; McDonald et al., 2014; Gately and Hutyra, 2017). Gately et al. (2013) pointed out, that based on the road density proxy a downscaling of total US emissions leads to an overestimation of on-road emissions for areas with higher than average road densities (and vice versa). Also in the study by McDonald et al. (2014) vehicle emissions were overestimated by 40 to 80% in Californian cities. We are not aware of similar studies for European cities. While there is a strong seasonality of CO_2 fluxes due to domestic heating (with its emission maximum in winter), the contribution from road traffic (the second most important CO_2 sector for this study according to the inventories, see **Table 3**) is relatively constant throughout the year (Kuc et al., 2003; Gioli et al., 2012; EDGAR monthly resolved emissions in 2010). As a consequence, inventorial CO_2 fluxes in summer are expected to be lower than presented in **Figure 7**. Thus, probing Berlin during different seasons would be very valuable.

Hase et al. (2015) reports on urban Berlin emissions apparent in XCO_2 signals (column-averaged dry air mole fraction) from five ground-based Bruker EM27/SUN Fourier-Transform infrared (FTIR) spectrometers. Applying a simple dispersion model for three measurement days in June and July 2014 they retrieve a CO_2 source strength of 0.8 t s^{-1}. Compared to the estimate of Hase et al. (2015), our flux estimate is almost twice as large, but agrees well within the error estimate. Our stronger emission rate is not surprising, as measurements were performed four years apart and CO_2 emissions have a very strong seasonal and diurnal cycle. In addition, due to the fixed location of FTIR spectrometers, emission rates might have been estimated from a different (possibly smaller) footprint area, which would result in lower emission rates.

In the temperate latitudes the CO_2 uptake of plants usually predominates in spring and summer. A modelling study using synthetic CO_2 data by Mueller et al. (2018) showed, that for the Baltimore-Washington area a substantial fraction of ~35% of the CO_2 background variability is caused by biogenic sources and sinks in July.

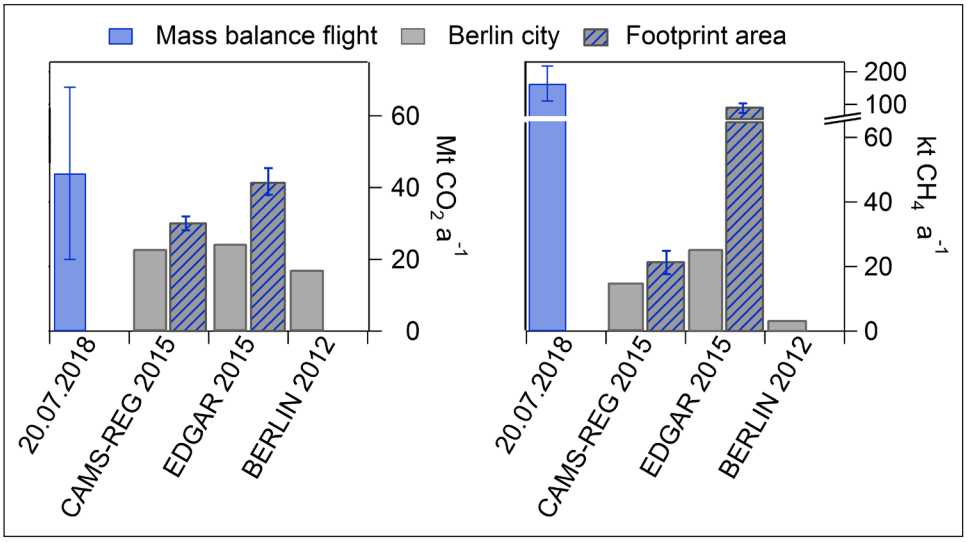

Figure 7: GHG emission fluxes for the Berlin area. Estimated mass balance fluxes for CO_2 (left) and CH_4 (right) from the flight on July 20th in blue. Grey bars indicate inventorial fluxes within the Berlin city boundary. Striped bars represent the inventory fluxes enlarged by the area from the corresponding footprint analysis. DOI: https://doi.org/10.1525/elementa.411.f7

Therefore, we simulate the biogenic CO_2 flux with the Vegetation Photosynthesis and Respiration Model (VPRM, Mahadevan et al., 2008) coupled with WRF-GHG (Beck et al, 2013) in order to estimate the influence of the photosynthetic uptake and respiration on our assessment of the anthropogenic flux. According to our analysis, the maximum daytime photosynthetic uptake predicted over the footprint area is at most 12% of the estimated anthropogenic flux. Due to that and the fact that the change of the predicted CO_2 biogenic signal over the small constrained area is low (well within the observed variability of the signal), we have concluded that the explicit correction for the biogenic influence is not needed. More information can be found in the supplement (see Figure S6 and the discussion therein). Hardiman et al. (2017) simulates the biogenic carbon flux throughout Massachusetts, including the urban area Boston, by using the VPRM model, which was specifically adapted to urban-specific influences by e.g. incorporating higher temperatures and impervious surfaces like pavement and buildings. They conclude that urban vegetation is probably not offsetting a significant fraction of anthropogenic emissions (e.g. only ~2% in Boston), which is consistent with previous studies cited therein.

In contrast to the observed CO_2 plume pattern, the CH_4 plume extended further to the west over the city limits. Also the XCH_4 signal of Hase et al. (2015) did not follow their XCO_2 pattern (due to different sources), and a distinct background could not be observed. Compared to the footprint-corrected inventorial data, our annual CH_4 flux estimate of ~164 ± 54 kt a^{-1} is tremendously larger (factor ~7) than the CAMS-REG estimate, which has only little contribution of the waste sector. However, it agrees better with EDGAR, which considers larger emission amounts coupled to any form of waste treatment (for source sector partitioning see **Table 3**). According to Saunois et al. (2016), CH_4 produced in waste water is dependent on the amount of organic content in the water itself. The inventories considered in their study (EDGAR v.42FT2010, GAINS 5a, USEPA 2012) give global emissions from waste water in the range of 9 to 30 Tg in 2005 (3 to 9% of global anthropogenic emissions). For the greater area of Berlin, EDGAR even states that 18% of total emissions are related to waste water handling and 48% to solid waste deposition. In London, waste treatment and disposal is the primary source of CH_4 based on the National Atmospheric Emissions Inventory besides natural gas leakage (Pitt et al., 2019). As ethane (C_2H_6) is co-emitted with CH_4 in oil and gas operations, we can use it as a tracer for gas leakages. However, during our mission flights we did not detect any significant variations in the QCLS C_2H_6 data. When comparing total CH_4 emissions from Germany, CAMS-REG is only a factor of 0.4 lower than EDGAR (and both inventories agree for CO_2) as both inventories are scaled to fit to the reported country values. As a result, we conclude that the waste sector (SNAP 9) in CAMS-REG is most likely underrepresented in the Berlin area either in terms of strength or in terms of spatial distribution, or a combination of both.

3.3 Comparison of GHG measurements with the MECO(n) simulation results

With the high-resolution numerical model MECO(n) of ~1 km × 1 km we simulate CO_2 and CH_4 mixing ratios based on different source tracers (as described in Sect. 2.3.2). By comparing the model output to our airborne measurements, we aim to better understand the source sectors and regions contributing to the measured pollution plumes. Note that in the MECO(n) model simulations the potential temporal source strength variability (on daily, weekly or seasonal timescales) cannot be captured, as only annual averaged emissions from the prescribed inventories are available.

3.3.1 Underestimated and missing CH_4 sources as observed on July 20th

For the flight on July 20th (as described in Sect. 3.2) backward trajectories were started from the location of the CO_2 plume. They cover the entire city of Berlin and the estimated CO_2 mass flux is in agreement with current inventories. In contrast, backward trajectories released from the broader CH_4 plume, which extend over the city boundary, indicate an impact of emissions from further west of the city and a relatively large CH_4 emission flux was derived.

In a first step we simulate GHG mixing ratios based on the local BERLIN inventory to isolate the urban emissions (called c-CO_2 and c-CH_4 for "city", see **Table 2**). Please note, that due to the model biases (as discussed below) MECO(n) in the applied setup is able to provide spatial distributions for the two GHG, but is limited in the representation of absolute values. In **Figure 8** different perspectives are presented. Panels (a) and (b) show the 2D distribution of simulated column-averaged dry air mole fraction at 13 UTC to illustrate the plume extent. Panel (c) depicts on the right axis the simulated GHG mixing ratios (indicated in grey), which have been sampled on-line along the flight track (submodel S4D as described by Jöckel et al., 2010). Together with the measured GHG enhancements on the left axis, the GHG distribution along the horizontal distance of the flight track is shown. The measured enhancements refer to the upwind mixing ratios being subtracted from the observed downwind mixing ratios and are indicated in dark red. The average measured wind direction during the flight was 299 ± 27°. The MECO(n) results reflect the prevalent wind direction quite well with 305 ± 36°, therefore the location of the simulated c-CO_2 plume agrees well with the measured CO_2 plume. In addition, the shape of the simulated plume is consistent with observations and also the coherent c-CO_2 mixing ratios within all heights. However, the maximum enhancements differ by a factor of ~2. This is either the result from underestimated prescribed emissions, or coupled to any form of model biases (or a combination of both). A quantitative comparison of maximum enhancements is difficult due to large differences in simulated wind speed (+2.1 m s^{-1}) compared to observations, thus reducing the enhancement. Furthermore, differences in the simulated PBL depth (~600 m lower than observed) influence the GHG dilution within the PBL and increase the enhancement,

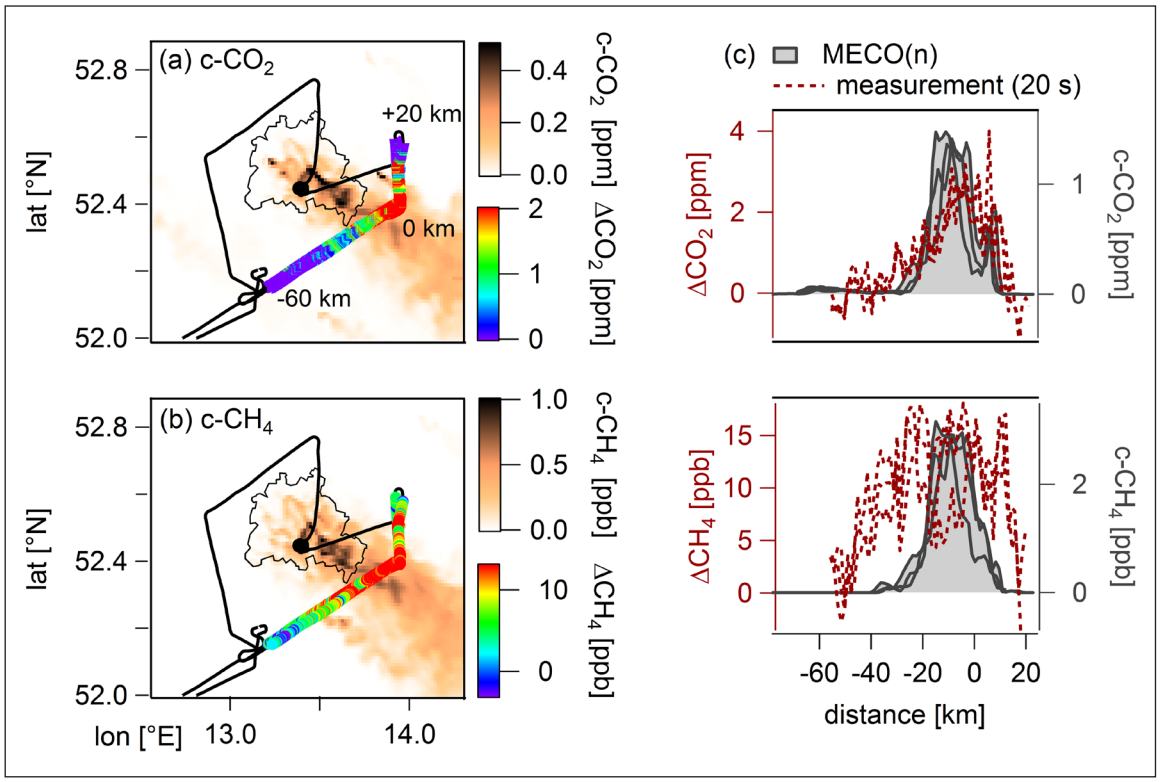

Figure 8: Simulated and measured GHG mixing ratios on July 20th. 2D distributions of simulated column-averaged dry air mole fractions of **(a)** the c-CO_2 and **(b)** the c-CH_4 tracer at 13 UTC of July 20th. The flight path is shown in black, and the downwind "wall" is colour-coded according to the measured CO_2 and CH_4 enhancement. Panel **(c)** presents GHG mixing ratios along the horizontal distance (simulated mixing ratios in grey; GHG measurements, averaged on the model time resolution of 20 s, in dark red). DOI: https://doi.org/10.1525/elementa.411.f8

but also affect the plume width. Emissions from the point sources east of Berlin (see **Figure 6a**), which are reflected by the sharp CO_2 measurement spikes at ~7 km distance, are clearly visible at ~52.5°N and ~13.8°E, as well as in the simulated c-CO_2 mixing ratio along the flight track.

With respect to simulated c-CH_4 (grey) and measured CH_4 (dark red), it stands out that simulated c-CH_4 enhancements are far too low (factor of ~5), although the BERLIN inventory is already scaled with a factor of ~4.5 (see **Table 2**) and the observed plume is significantly wider. This implies a huge underestimation of urban source strengths in the BERLIN inventory, or missing CH_4 emissions in the surroundings of Berlin. One should keep in mind that CO_2 observations are reflected by the simulated city emissions quite well. Thus, a number of different tracers were implemented, in order to investigate the origin of the unexpected missing CH_4 sources which are required to reproduce the observed CH_4 pattern.

The outer parts of the plume could not be reproduced by the "regional" tracer r-CH_4 (coupled CAMS-REG inventory; not shown), therefore we did further studies to examine the contribution from emissions of the waste sector to the detected CH_4 plume. **Figure 9** depicts simulated CH_4 mole fractions from the tracers related to waste water treatment plants (w-CH_4, panel a), landfills (l-CH_4, panel b) and to the combined tracer t-CH_4 (which is "city" plus "waste water" plus "landfills", panel c). Largest waste water facilities (they are sized according to their population equivalent) are located directly outside of the city; smaller facilities are found more frequently in the west and south-west and produce a rather homogenous CH_4 mole fraction distribution field, despite their nature of point sources. Simulated CH_4 mole fractions from the landfill tracer (information according to CORRECTIV, 2016) indicate more point-like distributions of enhanced CH_4 either from waste-rich dumps (they are sized according to the amount of deposited waste) or from a spatial concentration of several dumps, e.g. seen in the north of Berlin. **Figure 9c** shows the mole fractions from the combined t-CH_4 tracer. As already stated in Sect. 2.4, we do not claim that our emission rate estimate for waste water and landfills are correct, however, the inhomogeneous CH_4 distribution, resulting from the t-CH_4 tracer, is consistent with the results of Hase et al. (2015), who report a less uniform and more varying CH_4 background compared to CO_2. The mean mixing ratio from the three altitude transects for each tracer (w-CH_4, l-CH_4, and t-CH_4) is shown in **Figure 9d** along the horizontal distance of the flight path together with the measured CH_4 enhancement (mean of the lower two flight transects only). Although these model results do not directly reproduce the measured CH_4 plume shape, emissions from waste water plants and landfills contribute (broaden and enhance) to the simulated c-CH_4 plume (see **Figure 8c**), which considers only the city emissions. These results suggest that for a better understanding of the regional CH_4 budget, emission strengths from these

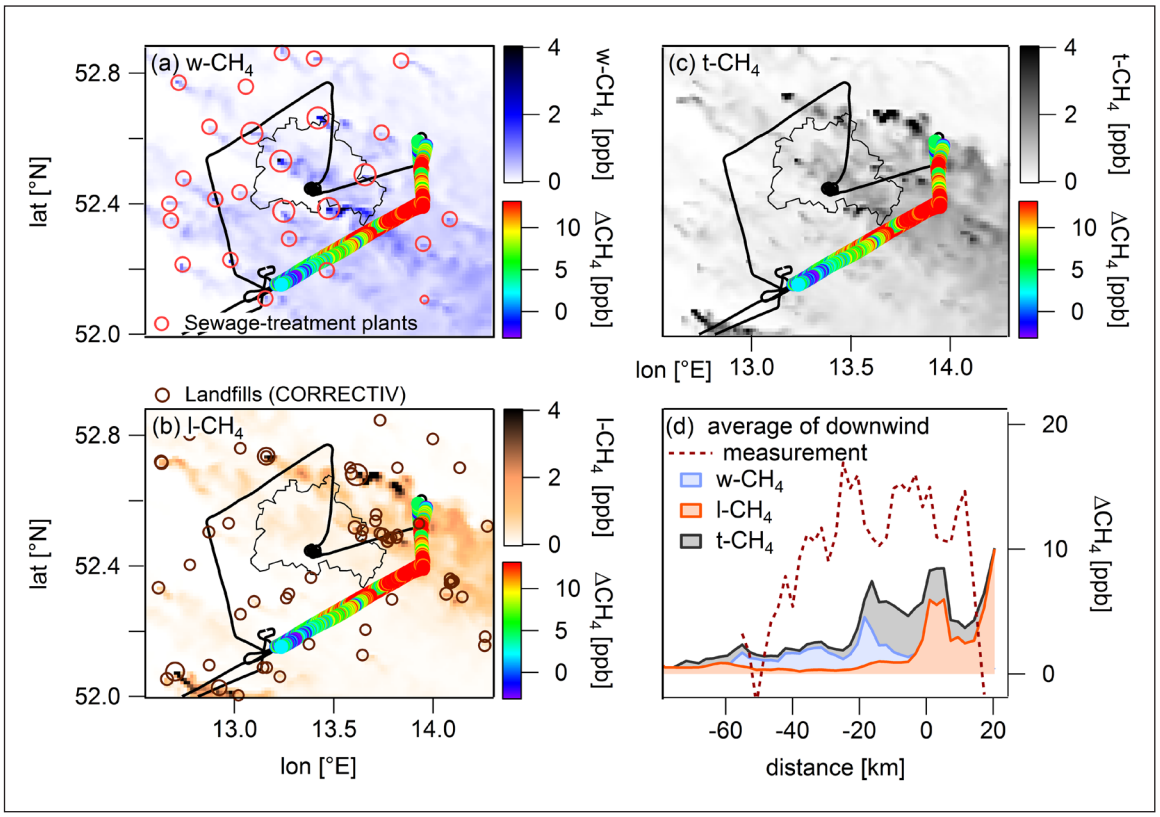

Figure 9: Simulated and measured CH_4 mixing ratios on July 20th. 2D distributions of simulated column-averaged dry air mole fractions of **(a)** the w-CH_4, **(b)** the l-CH_4, and **(c)** the t-CH_4 tracer at 13 UTC of July 20th. The flight path is shown in black, and the downwind "wall" is colour-coded according to the measured CH_4 enhancement. Panel **(d)** presents the average GHG mixing ratios along the flown horizontal distance. For the simulated mixing ratios based on the three tracers (w-CH_4 in blue, l-CH_4 in orange and t-CH_4 in black) all three flight transects are considered. For the averaged measured CH_4 enhancement (dark red) only the lower two flight transects are taken. DOI: https://doi.org/10.1525/elementa.411.f9

sources need to be experimentally verified by e.g. a ground based measurement campaign in the greater region of Berlin.

3.3.2 Greenhouse gas plume as observed on July 24th

From the results of Sect. 3.3.1 two hypotheses can be formulated. First, the reported urban CO_2 emissions from Berlin are well constrained, since the simulated c-CO_2 enhancements are in the same order of magnitude as our measured CO_2 enhancements. Second, and in contrast, the reported urban CH_4 emissions are largely underestimated. Based on this single research flight we were able to show, that simulated c-CH_4 enhancements are dramatically smaller than our measured CH_4 enhancements. To analyse the robustness of our hypothesis in more detail, we compare observations from an additional flight performed on July 24th (see **Table 4)** with the MECO(n) simulated GHG mixing ratios.

The time series of the whole flight (~12:10 to ~15:00 UTC) can be found in Figure S1. **Figure 10a** shows measured CO_2 (upper panel) and CH_4 (lower panel) mixing ratios of the three downwind transects along the horizontal distance. The flight track is depicted in **Figure 10b** and **c** together with the simulated full atmospheric column-averaged dry air mole fractions from the c-CO_2 and c-CH_4 tracer, respectively. The flight pattern is constructed similar to the one on July 20th with an upwind transect (at 796 m) and a vertical profile at the Tempelhofer Feld (~0.3 to ~3.2 km; ascend rate of ~3.1 m s^{-1}). We sampled the plume at three altitudes (494, 827 and 1308 m) starting from 0 km distance towards the east (indicated with positive distances). Instead of forecasted northern winds (E-W alignment of the flight transects), the wind was blowing from the NNE with 3.3 m s^{-1} on average. To aim for sampling background air, the transects were prolonged towards the NW (negative distance; determined by restrictions from ATC).

As obvious in **Figure 10a**, CO_2 and CH_4 mixing ratios were enhanced above the background by up to 5 ppm CO_2 and 18 ppb CH_4, respectively. As seen in the comparable CO_2 mixing ratios at all heights, the PBL is generally well-mixed (which is consistent with the meteorological vertical profile, see Figure S2). Measured CH_4 mixing ratios are coherent in the two lower flight transects, however, show a different pattern at the highest altitude with a dip in CH_4 between ~20 and ~30 km (similar to observations on July 20th, see Sect. 3.2.1). Furthermore, the encountered GHG plume can be divided into two parts, with a positive correlation between CO_2 and CH_4 in the middle and eastern part (R = +0.82) and slightly negative correlations in the north-western part (R = –0.20). The dashed lines in **Figure 10a** indicate the linear interpolated background

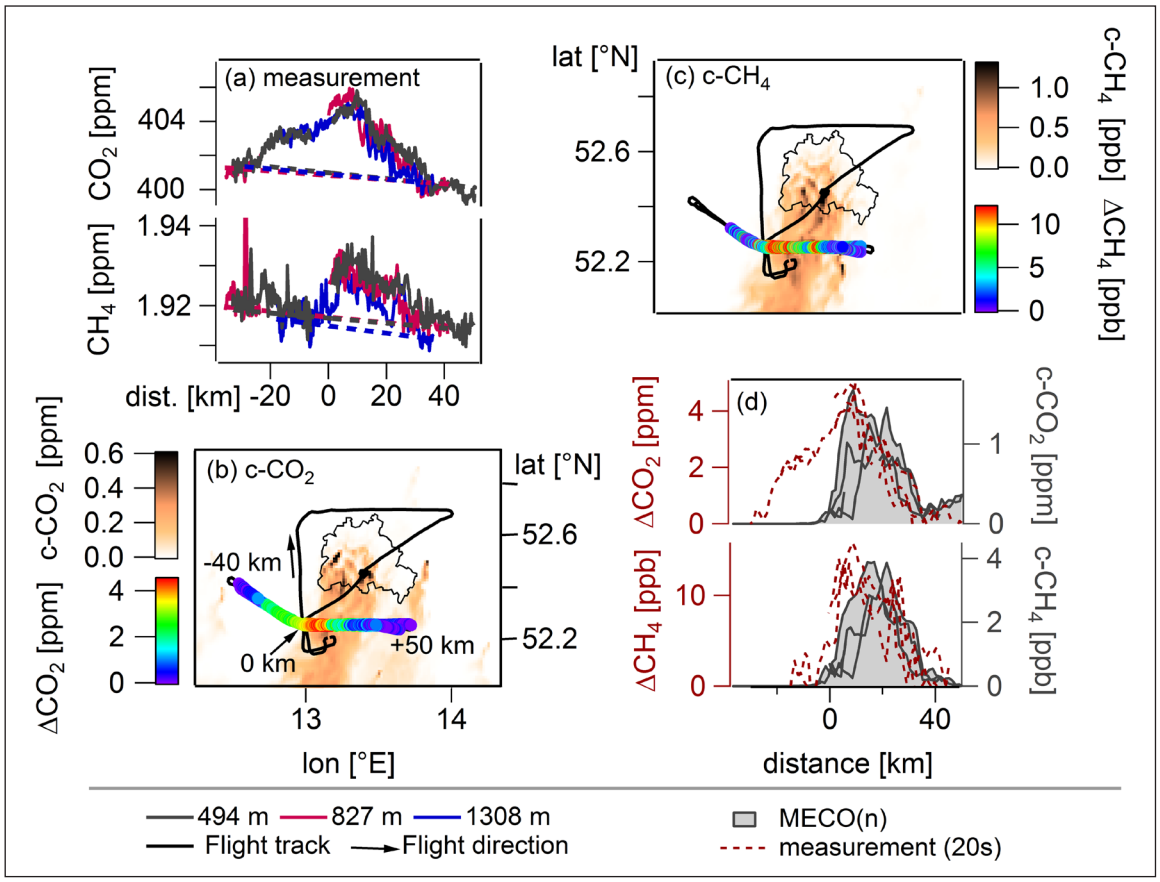

Figure 10: Measured and simulated GHG mixing ratios on July 24th. (a) Measured CO_2 (upper panel) and CH_4 (lower panel) mixing ratios (segment mean) on July 24th of the three downwind transects along the horizontal distance. The linearly interpolated background is indicated by the dashed line. Panel **(b)** and **(c)** show the 2D distributions at 14 UTC of the simulated column-averaged dry air mole fractions of the c-CO_2 and c-CH_4 tracer, respectively. The flight path is drawn in black and the downwind "wall" is colour-coded according to the measured CO_2 and CH_4 enhancement. Panel **(d)** presents GHG mixing ratios along the horizontal distance (simulated mixing ratios in grey; observed GHG mixing ratios which are averaged to the models resolution of 20 s in dark red). DOI: https://doi.org/10.1525/elementa.411.f10

mixing ratios based on the edges of the flight track. GHG mixing ratios in the eastern part are lower than in the western part (~1.5 ppm for CO_2 and ~4 to ~6 ppb for CH_4).

We refrain from estimating GHG fluxes based on the mass balance approach for this second case study, because our analyses indicates that due to very low wind speeds emissions accumulated above Berlin during the night and in the morning of July 24th (see Sect. S5 and S6 in the supplement for more details). Steady winds are, however, essential for the mass balance approach.

The simulated column-averaged dry air mole fractions from the c-CO_2 and c-CH_4 tracer at 14 UTC are presented in **Figure 10b** and **c**, respectively. The downwind "wall" is colour-coded according to the measured enhancement (here the linear background is subtracted from the observed downwind mixing ratios). **Figure 10b** indicates that the simulated c-CO_2 plume only captures the eastern part of the detected plume, although the simulated wind direction is similar to the measured wind direction (+2°). The mixing ratios along the flight track are depicted in **Figure 10d** (from the c-CH_4 and c-CO_2 tracer in grey on the right axis, from the airborne measurements in dark red on the left axis). This depiction confirms that the eastern part of the CO_2 plume is well captured by c-CO_2, however, the western part is missing. Neither in the EDGAR inventory, nor in E-PRTR any strong source of CO_2 is present west of Berlin (or within western Berlin), which could explain our observations. Also in the simulated mixing ratio from the r-CO_2 tracer (coupled regional CAMS-REG inventory; not shown) we could not reproduce this part of the plume. However, the disagreement in the plume shape possibly might arise from a transport and/or timing bias in the MECO(n) simulation. The time-series of the simulated GHG plume on the 24th of July shows, that the plume meanders from east to west, i.e. already at 16 UTC the plume is located more in the west (see Figure S11 in the supplement). However, the simulated maximum c-CO_2 enhancement of ~2 ppm is 2 to 3 times lower than our measured enhancement of ~5 ppm. MECO(n) simulates a higher PBL depth (~200 m) and overestimates the wind speed (+2.6 m s^{-1}), thus leading to simulated GHG mixing ratios which are much more diluted within the PBL. Although this dilution cannot be properly quantified, we can deduce that the order of magnitude of simulated c-CO_2 mixing ratios is in much better agreement with our measurements than it is the case for CH_4, similar to the

results from the flight on July 20th. The lower panel of **Figure 10d** indicates that the plume structure of c-CH_4 is well simulated, as well as the coherent mixing ratios at all heights. The maximum simulated enhancement of only ~4 ppb is, however, heavily underestimated (factor 4 to 5).

4 Conclusion

An improved understanding and quantification of the GHG budget is needed for the development of efficient mitigation strategies and for the prediction of future climate impacts. With our study we contribute to the sparse knowledge of GHG emissions from European cities by studying the urban CO_2 and CH_4 distribution downwind of the German capital Berlin. Emission inventories available for Berlin (EDGAR, CAMS-REG and BERLIN) differ by a factor of ~1.4 and ~8 for CO_2 and CH_4, respectively.

In July 2018 we performed in situ CO_2 and CH_4 measurements aboard the DLR Cessna Grand Caravan in the outflow of Berlin to assess the urban GHG emissions from the city. Our measurements showed, that even with sensitive airborne in-situ measurements it remains challenging to detect Berlins GHG emissions, which fits to the observations reported by Hase et al. (2015) who used ground-based FTIR spectrometer measurements, and by Kuhlmann et al. (2019a) who used synthetic CO_2 satellite observations.

The detection and isolation of the urban GHG plume, however, was possible during two research flights performed on July 20th and July 24th. GHG enhancements were observed in different heights of a well-mixed and efficiently capped boundary layer. Using the mass balance approach, we obtained a CO_2 flux of 1.39 ± 0.76 t s^{-1} for the flight on July 20th, which is in the same order of magnitude as the numbers given in the presented inventories. Sampled air masses homogenously passed the city of Berlin prior to our measurement, where they were enriched with emissions. Simulated citywide CO_2 mixing ratios agree well with our CO_2 measurements in location and shape, while a quantitative comparison of simulated and measured maximum enhancements is hampered due to deviations in the wind speed and PBL depth.

For the same flight we calculated a CH_4 mass flux of 5.20 ± 1.70 kg s^{-1}, which is almost two times larger than the highest reported value in the inventories (i.e. the footprint-corrected estimate from EDGAR). Simulated citywide CH_4 mixing ratios were substantially lower than observed as well, indicating a significant underrepresentation of urban emissions in the local BERLIN and regional CAMS-REG inventory. The CH_4 plume (in contrast to the CO_2 plume) partly originated also from outside of the Berlin city boundary. Our study shows that emissions potentially originate from sources surrounding the city, which are missing in the three investigated inventories. These might include emissions from waste water treatment plants and illegal landfills as indicated by information from other sources. However, for a clear attribution to these sources, a verification of these emissions is required by ground-based measurements and/or further airborne in-situ observations.

Although Berlin can be considered as a relatively isolated city (especially for the densely populated region of Central Europe), we demonstrated the need for precisely determining the inflow GHG mixing ratios and the natural variability of the background concentrations in order to suitably apply the mass balance approach. One possibility to improve the estimation of the background is to sample the upwind and downwind transects in a Lagrangian manner, e.g. also using two aircraft simultaneously. To further improve the knowledge on the regional CH_4 budget in the greater Berlin area, subsequent measurement campaigns are needed with a special focus on emission sources located outside the city boundaries. Furthermore, different seasons should be investigated to reflect the seasonal cycle of the emissions.

Our study showed that bottom-up CO_2 and, in particular, CH_4 emission inventories are subject to large uncertainties at the city scale, even for major cities in highly developed countries like Germany, and that top-down emission estimates are an important tool to verify emission estimates and to reveal missing sources in emission inventories.

Data Accessibility Statement

Observational data (https://doi.org/10.5281/zenodo.3706725; Klausner et al, 2020) and simulation results (https://doi.org/10.5281/zenodo.3707990; Mertens and Jöckel, 2020) are publicly available. The MECO(n) model system is part of the Modular Earth Submodel System (MESSy). MESSy is continuously further developed and applied by a consortium of institutions. The usage of MESSy and access to the source code is licenced to all affiliates of institutions which are members of the MESSy Consortium. Institutions can become a member of the MESSy Consortium by signing the MESSy Memorandum of Understanding. The COSMO model, as part of MECO(n), is licenced by the German Weather Service (DWD), or by the COSMO-CLM community. More information can be found on the MESSy Consortium Website (http://www.messy-interface.org). The code used for the present study has been based on MESSy version 2.54.0.

Supplemental files

The supplemental files for this article can be found as follows:

- **Figure S1.** Time series of CO_2, CH_4 and flight altitude for five research flights during July 2018. DOI: https://doi.org/10.1525/elementa.411.s1
- **Figure S2. Vertical profiles of the upward spiral at Tempelhofer Feld.** The PBL depth (dashed black line) was determined from virtual potential temperature, static temperature and relative humidity. DOI: https://doi.org/10.1525/elementa.411.s1
- **Figure S3. Aerosol lidar measurements at Leipzig.** The temporal evolution of the range-corrected signal at 1064 nm is shown. Available at http://polly.tropos.de/?p=lidarzeit&Ort=1&Jahr=2018. Accessed October 04, 2019. Further information can be found in Engelmann et al. (2016) and Baars et al. (2016). DOI: https://doi.org/10.1525/elementa.411.s1
- **Figure S4. Time series of forecasted and actual wind direction and wind speed.** The whole cam-

paign period from July 8th to 26th is shown. DOI: https://doi.org/10.1525/elementa.411.s1

- **Figure S5. Correlations of wind direction and wind speed between airborne measurement data and ECMWF forecast data.** Correlation coefficients are abbreviated with Pr. DOI: https://doi.org/10.1525/elementa.411.s1
- **Figure S6.** Biogenic CO_2 mixing ratios up- and downwind of Berlin on July 20th. DOI: https://doi.org/10.1525/elementa.411.s1
- **Figure S7. Ascents of a captive balloon system located at Tempelhofer Feld on July 24th.** Wind measurements were carried out by the DWD (R. Becker, P. Stanislawsky, M. Koßmann) in the framework of the $[UC]^2$ project. DOI: https://doi.org/10.1525/elementa.411.s1
- **Figure S8. Backward trajectory calculations for July 24th.** Trajectories were started at 14:30 UTC from the downwind flight track backwards in time for 6 hours. Colour coded is the height of the trajectory according to its relative position. DOI: https://doi.org/10.1525/elementa.411.s1
- **Figure S9. Population density for Berlin and the state Brandenburg from 2017.** The yellow to red colours indicate the inhabitants per km^2, the blue dots show numbers for total population in each municipality. The Berlin city boundary (black) was added as well as latitude and longitude labels. Adapted after Strukturatlas Land Brandenburg (2017). DOI: https://doi.org/10.1525/elementa.411.s1
- **Figure S10. Curtain of simulated c-CH_4 and c-CO_2 on July 20th.** The third crossing of the Berlin plume at ~1600 m altitude is shown from ~13:20 to ~13:35 UTC. DOI: https://doi.org/10.1525/elementa.411.s1
- **Figure S11. Time-series of the simulated c-CO_2 plume on July 24th.** Shown are snapshots at (a) 14 UTC, which is identical to Figure 10b and (b) at 16 UTC to indicate, that the plume moves towards the west during the afternoon. DOI: https://doi.org/10.1525/elementa.411.s1
- **Text S1.** Calibration procedure and measurement uncertainty. DOI: https://doi.org/10.1525/elementa.411.s1
- **Text S2.** Greenhouse gas time series and altitude profiles. DOI: https://doi.org/10.1525/elementa.411.s1
- **Text S3.** ECMWF forecast data and wind measurement agreement. DOI: https://doi.org/10.1525/elementa.411.s1
- **Text S4.** Biogenic CO_2 flux. DOI: https://doi.org/10.1525/elementa.411.s1
- **Text S5.** Wind situation on July 24th. DOI: https://doi.org/10.1525/elementa.411.s1
- **Text S6.** Backward trajectories on July 24th. DOI: https://doi.org/10.1525/elementa.411.s1
- **Text S7.** Berlin and its surrounding area. DOI: https://doi.org/10.1525/elementa.411.s1
- **Text S8.** Simulated vertical GHG distribution within the PBL. DOI: https://doi.org/10.1525/elementa.411.s1

Acknowledgements

The authors especially thank Paul Stock, Monika Scheibe and Julian Kostinek from DLR-IPA for their engineering support. Furthermore, we thank DLR-FX for the campaign cooperation, especially the pilots Thomas van Marwick and Klaus Dietl and the group of Ralph Helmes, Kevin Raynor, Andreas Giez, Martin Zöger, Martin Sedlmeir, Florian Gebhardt and Christian Mallaun. A special thanks is dedicated also to the 3DO project partner for their cooperation, and especially to Ralf Becker, Peter Stanislawsky and Meinolf Koßmann from the DWD for processing and providing additional wind data. Finally, we are very grateful to Andreas Kerschbaumer (Senatsverwaltung Berlin) for providing the emission inventory of Berlin.

Funding information

We thank DLR VO-R for funding the young investigator research group "Greenhouse Gases". The German Federal Ministry of Education and Research (BMBF) funds the 3DO consortium under grant 01LP1602 within the framework of Research for Sustainable Development (FONA; www.fona.de). The German Aerospace Center (DLR) Project Management Agency supports the consortium. We further acknowledge funding from the Initiative and Networking Fund of the Helmholtz Association through the project "Advanced Earth System Modelling Capacity (ESM)". Computational resources for the simulation were provided by the German Climate Computing Centre (DKRZ) in Hamburg (project 0617). Michal Galkowski and WRF-GHG simulations were supported by the BMBF through AIRSPACE (FK 01LK1701C). The computations were performed at the DKRZ.

Competing interests

The authors have no competing interests to declare.

Author contributions

- Contributed to conception and design: TK, AR, HH
- Contributed to acquisition of data: TK, MM, MG, GK, RB, AF, PJ, MP
- Contributed to analysis and interpretation of data: TK, MM, HH, MG, GK, RB, AF, PJ, MP, AR
- Drafted and/or revised the article: TK, MM, HH, MG, GK, RB, AF, PJ, MP, AR
- Approved the submitted version for publication: TK, MM, HH, MG, GK, RB, AF, PJ, MP, AR

References

AVISO GmbH and **IE Leipzig.** 2016. Erstellung der Berliner Emissionskataster Industrie, Gebäudeheizung, sonstiger Verkehr, Kleingewerbe, sonstige Quellen, Baustellen – Schlussbericht Juni 2016. *Techn. rep.* Available at https://www.berlin.de/senuvk/umwelt/luftqualitaet/de/emissionen/download/Endbericht_Emissionkataster_2015.pdf. Accessed September 30, 2019.

Beck, V, Gerbig, C, Koch, T, Bela, MM, Longo, KM, Freitas, SR, Kaplan, JO, Prigent, C, Bergamaschi, P and **Heimann, M.** 2013. WRF-Chem simulations in the Amazon region during wet and dry

season transitions. Evaluation of methane models and wetland inundation maps. *Atmos Chem Phys* **13**(16): 7961–7982. DOI: https://doi.org/10.5194/acp-13-7961-2013

Bergamaschi, P, Karstens, U, Manning, AJ, Saunois, M, Tsuruta, A, Berchet, A, Vermeulen, AT, Arnold, T, Janssens-Maenhout, G, Hammer, S, Levin, I, Schmidt, M, Ramonet, M, Lopez, M, Lavric, J, Aalto, T, Chen, H, Feist, DG, Gerbig, C, Haszpra, L, Hermansen, O, Manca, G, Moncrieff, J, Meinhardt, F, Necki, J, Galkowski, M, O'Doherty, S, Paramonova, N, Scheeren, HA, Steinbacher, M and **Dlugokencky, E.** 2018. Inverse modelling of European CH_4 emissions during 2006–2012 using different inverse models and reassessed atmospheric observations. *Atmos Chem Phys* **18**(2): 901–920. DOI: https://doi.org/10.5194/acp-18-901-2018

Brandt, AR, Heath, GA, Kort, EA, O'Sullivan, F, Pétron, G, Jordaan, SM, Tans, P, Wilcox, J, Gopstein, AM, Arent, D, Wofsy, S, Brown, NJ, Bradley, R, Stucky, GD, Eardley, D and **Harriss, R.** 2014. Methane leaks from North American natural gas systems. *Science* **343**(6172): 733–735. DOI: https://doi.org/10.1126/science.1247045

Bréon, FM, Broquet, G, Puygrenier, V, Chevallier, F, Xueref-Remy, I, Ramonet, M, Dieudonné, E, Lopez, M, Schmidt, M, Perrussel, O and **Ciais, P.** 2015. An attempt at estimating Paris area CO_2 emissions from atmospheric concentration measurements. *Atmos Chem Phys* **15**(4): 1707–1724. DOI: https://doi.org/10.5194/acp-15-1707-2015

Brunner, D, Kuhlmann, G, Marshall, J, Clément, V, Fuhrer, O, Broquet, G, Löscher, A and **Meijer, Y.** 2019. Accounting for the vertical distribution of emissions in atmospheric CO_2 simulations. *Atmos Chem Phys* **19**(7): 4541–4559. DOI: https://doi.org/10.5194/acp-19-4541-2019

Cambaliza, MOL, Shepson, PB., Bogner, J, Caulton, DR, Stirm, B, Sweeney, C, Montzka, SA, Gurney, KR, Spokas, K, Salmon, OE, Lavoie, TN, Hendricks, A, Mays, K, Turnbull, J, Miller, BR, Lauvaux, T, Davis, K, Karion, A, Moser, B, Miller, C, Obermeyer, C, Whetstone, J, Prasad, K, Miles, N and **Richardson, S.** 2015. Quantification and source apportionment of the methane emission flux from the city of Indianapolis. *Elementa: Science of the Anthropocene* **3**(37). DOI: https://doi.org/10.12952/journal.elementa.000037

Cambaliza, MOL, Shepson, PB, Caulton, DR, Stirm, B, Samarov, D, Gurney, KR, Turnbull, J, Davis, KJ, Possolo, A, Karion, A, Sweeney, C, Moser, B, Hendricks, A, Lauvaux, T, Mays, K, Whetstone, J, Huang, J, Razlivanov, I, Miles, NL and **Richardson, SJ.** 2014. Assessment of uncertainties of an aircraft-based mass balance approach for quantifying urban greenhouse gas emissions. *Atmos Chem Phys* **14**(17): 9029–9050. DOI: https://doi.org/10.5194/acp-14-9029-2014

Chen, H, Winderlich, J, Gerbig, C, Hoefer, A, Rella, CW, Crosson, ER, van Pelt, AD, Steinbach, J, Kolle, O, Beck, V, Daube, BC, Gottlieb, EW, Chow, VY, Santoni, GW and **Wofsy, SC.** 2010. High-accuracy continuous airborne measurements of greenhouse gases (CO_2 and CH_4) using the cavity ring-down spectroscopy (CRDS) technique. *Atmos Meas Tech* **3**(2): 375–386. DOI: https://doi.org/10.5194/amt-3-375-2010

CORRECTIV. 2016. Available at https://correctiv.org/artikel/2016/03/02/muellparadies-brandenburg. Accessed August 18, 2019.

Crippa, M, Solazzo, E, Huang, G, Guizzardi, D, Koffi, E, Muntean, M, Schieberle, C, Friedrich, R and **Janssens-Maenhout, G.** 2019. High resolution temporal profiles in the Emissions Database for Global Atmospheric Research (EDGAR). *Nature Scientific Data*. Submitted.

Dlugokencky, EJ. 2005. Conversion of NOAA atmospheric dry air CH_4 mole fractions to a gravimetrically prepared standard scale. *J Geophys Res* **110**(D18): 273. DOI: https://doi.org/10.1029/2005JD006035

EPA. 2010. Available at https://www3.epa.gov/ttnchie1/efpac/ghg/GHG_Biogenic_Report_draft_Dec1410.pdf. Accessed August 18, 2019.

Gately, CK and **Hutyra, LR.** 2017. Large Uncertainties in Urban-Scale Carbon Emissions. *J Geophys Res-Atmos* **122**(20): 11242–11260. DOI: https://doi.org/10.1002/2017JD027359

Gately, CK, Hutyra, LR, Wing, IS and **Brondfield, MN.** 2013. A bottom up approach to on-road CO_2 emissions estimates: Improved spatial accuracy and applications for regional planning. *Environ Sci Technol* **47**(5): 2423–2430. DOI: https://doi.org/10.1021/es304238v

Gioli, B, Carfora, MF, Magliulo, V, Metallo, MC, Poli, AA, Toscano, P and **Miglietta, F.** 2014. Aircraft mass budgeting to measure CO_2 emissions of Rome, Italy. *Environ Monit Assess* **186**(4): 2053–2066. DOI: https://doi.org/10.1007/s10661-013-3517-4

Gioli, B, Toscano, P, Lugato, E, Matese, A, Miglietta, F, Zaldei, A and **Vaccari, FP.** 2012. Methane and carbon dioxide fluxes and source partitioning in urban areas: The case study of Florence, Italy. *Environ Pollut* **164**: 125–131. DOI: https://doi.org/10.1016/j.envpol.2012.01.019

Hardiman, BS, Wang, JA, Hutyra, LR, Gately, CK, Getson, JM and **Friedl, MA.** 2017. Accounting for urban biogenic fluxes in regional carbon budgets. *The Science of the total environment* **592**: 366–372. DOI: https://doi.org/10.1016/j.scitotenv.2017.03.028

Hartmann, DL, Klein Tank, AMG, Rusticucci, M, Alexander, LV, Brönnimann, S, Charabi, Y, Dentener, FJ, Dlugokencky, EJ, Easterling, DR, Kaplan, A, Soden, BJ, Thorne, PW, Wild, M and **Zhai, PM.** 2013. Observations: Atmosphere and Surface. In: *Climate Change 2013: The Physical Science Basis. Contribution of Working Group I to the Fifth Assessment Report of the Intergovernmental Panel on Climate Change,* Stocker, TF, Qin, D, Plattner, G-K, Tignor, M, Allen, SK, Boschung, J, Nauels, A, Xia, Y, Bex, V and Midgley, PM (eds.), 159–254. Cambridge,

United Kingdom and New York, NY, USA: Cambridge University Press. DOI: https://doi.org/10.1017/CBO9781107415324.008

Hase, F, Frey, M, Blumenstock, T, Groß, J, Kiel, M, Kohlhepp, R, Mengistu Tsidu, G, Schäfer, K, Sha, MK and **Orphal, J.** 2015. Application of portable FTIR spectrometers for detecting greenhouse gas emissions of the major city Berlin. *Atmos Meas Tech* **8**(7): 3059–3068. DOI: https://doi.org/10.5194/amt-8-3059-2015

Heimburger, AMF, Harvey, RM, Shepson, PB, Stirm, BH, Gore, C, Turnbull, J, Cambaliza, MOL, Salmon, OE, Kerlo, A-EM, Lavoie, TN, Davis, KJ, Lauvaux, T, Karion, A, Sweeney, C, Brewer, WA, Hardesty, RM and **Gurney, KR.** 2017. Assessing the optimized precision of the aircraft mass balance method for measurement of urban greenhouse gas emission rates through averaging. *Elementa: Science of the Anthropocene* **5**(26). DOI: https://doi.org/10.1525/elementa.134

Helfter, C, Famulari, D, Phillips, GJ, Barlow, JF, Wood, CR, Grimmond, CSB and **Nemitz, E.** 2011. Controls of carbon dioxide concentrations and fluxes above central London. *Atmos Chem Phys* **11**(5): 1913–1928. DOI: https://doi.org/10.5194/acp-11-1913-2011

Helfter, C, Tremper, AH, Halios, CH, Kotthaus, S, Bjorkegren, A, Grimmond, CSB, Barlow, JF and **Nemitz, E.** 2016. Spatial and temporal variability of urban fluxes of methane, carbon monoxide and carbon dioxide above London, UK. *Atmos Chem Phys* **16**(16): 10543–10557. DOI: https://doi.org/10.5194/acp-16-10543-2016

Hofmann, C, Kerkweg, A, Wernli, H and **Jöckel, P.** 2012. The 1-way on-line coupled atmospheric chemistry model system MECO(n) Part 3: Meteorological evaluation of the on-line coupled system. *Geosci Model Dev* **5**: 129–147. DOI: https://doi.org/10.5194/gmd-5-129-2012

Janssens-Maenhout, G, Pagliari, V, Guizzardi, D and **Muntean, M.** 2012. Global emission inventories in the Emission Database for Global Atmospheric Research (EDGAR). *Manual (I) – gridding: EDGAR emissions distribution on global gridmaps. Luxembourg: Publications Office* (EUR, Scientific and technical research series, 25785).

Jöckel, P, Kerkweg, A, Pozzer, A, Sander, R, Tost, H, Riede, H, Baumgaertner, A, Gromov, S and **Kern, B.** 2010. Development cycle 2 of the Modular Earth Submodel System (MESSy2). *Geosci Model Dev* **3**: 717–752. DOI: https://doi.org/10.5194/gmd-3-717-2010

Karion, A, Sweeney, C, Pétron, G, Frost, G, Michael Hardesty, R, Kofler, J, Miller, BR, Newberger, T, Wolter, S, Banta, R, Brewer, A, Dlugokencky, E, Lang, P, Montzka, SA, Schnell, R, Tans, P, Trainer, M, Zamora, R and **Conley, S.** 2013. Methane emissions estimate from airborne measurements over a western United States natural gas field. *Geophys Res Lett* **40**(16): 4393–4397. DOI: https://doi.org/10.1002/grl.50811

Kennedy, C, Demoullin, S and **Mohareb, E.** 2012. Cities reducing their greenhouse gas emissions. *Energ Policy* **49**: 774–777. DOI: https://doi.org/10.1016/j.enpol.2012.07.030

Kerkweg, A and **Jöckel, P.** 2012a. The 1-way on-line coupled atmospheric chemistry model system MECO(n) – Part 1: Description of the limited-area atmospheric chemistry model COSMO/MESSy. *Geosci Model Dev* **5**(1): 87–110. DOI: https://doi.org/10.5194/gmd-5-87-2012

Kerkweg, A and **Jöckel, P.** 2012b. The 1-way on-line coupled atmospheric chemistry model system MECO(n) – Part 2: On-line coupling with the Multi-Model-Driver (MMD). *Geosci Model Dev* **5**(1): 111–128. DOI: https://doi.org/10.5194/gmd-5-111-2012

Kirschke, S, Bousquet, P, Ciais, P, Saunois, M, Canadell, JG, Dlugokencky, EJ, Bergamaschi, P, Bergmann, D, Blake, DR, Bruhwiler, L, Cameron-Smith, P, Castaldi, S, Chevallier, F, Feng, L, Fraser, A, Heimann, M, Hodson, EL, Houweling, S, Josse, B, Fraser, PJ, Krummel, PB, Lamarque, J-F, Langenfelds, RL, Le Quéré, C, Naik, V, O'Doherty, S, Palmer, PI, Pison, I, Plummer, D, Poulter, B, Prinn, RG, Rigby, M, Ringeval, B, Santini, M, Schmidt, M, Shindell, DT, Simpson, IJ, Spahni, R, Steele, LP, Strode, SA, Sudo, K, Szopa, S, van der Werf, GR, Voulgarakis, A, van Weele, M, Weiss, RF, Williams, JE and **Zeng, G.** 2013. Three decades of global methane sources and sinks. *Nat Geosci* **6**(10): 813–823. DOI: https://doi.org/10.1038/ngeo1955

Klausner, T, Roiger, A, Fiehn, A, Giez, A, Dreiling, V, Zöger, M and **Mallaun, C.** 2020. Aircraft measurement data obtained within the framework of the 3DO measurement campaign in summer 2018 over Berlin. DOI: https://doi.org/10.5281/zenodo.3706725

Kostinek, J, Roiger, A, Davis, KJ, Sweeney, C, DiGangi, JP, Choi, Y, Baier, B, Hase, F, Groß, J, Eckl, M, Klausner, T and **Butz, A.** 2019. Adaptation and performance assessment of a quantum and interband cascade laser spectrometer for simultaneous airborne in situ observation of CH_4, C_2H_6, CO_2, CO and N_2O. *Atmos Meas Tech* **12**(3): 1767–1783. DOI: https://doi.org/10.5194/amt-12-1767-2019

Kuc, T, Rozanski, K, Zimnoch, M, Necki, JM and **Korus, A.** 2003. Anthropogenic emissions of CO_2 and CH_4 in an urban environment. *Appl Energ* **75**(3–4): 193–203. DOI: https://doi.org/10.1016/S0306-2619(03)00032-1

Kuenen, JJP, Visschedijk, AJH, Jozwicka, M and **van der Denier Gon, HAC.** 2014. TNO-MACC_II emission inventory, a multi-year (2003–2009) consistent high-resolution European emission inventory for air quality modelling. *Atmos Chem Phys* **14**(20): 10963–10976. DOI: https://doi.org/10.5194/acp-14-10963-2014

Kuhlmann, G, Broquet, G, Marshall, J, Clément, V, Löscher, A, Meijer, Y and **Brunner, D.** 2019b. Detectability of CO_2 emission plumes of cities and

power plants with the Copernicus Anthropogenic CO_2 Monitoring (CO_2M) mission. *Atmos Meas Tech* **12**: 6695–6719. DOI: https://doi.org/10.5194/amt-12-6695-2019

Kuhlmann, G, Clément, V, Marshall, J, Fuhrer, O, Broquet, G, Schnadt-Poberaj, C, Löscher, A, Meijer, Y and **Brunner, D.** 2019a. SMARTCARB – Use of Satellite Measurements of Auxiliary Reactive Trace Gases for Fossil Fuel Carbon Dioxide Emission Estimation, Final report of ESA study contract n°4000119599/16/NL/FF/mg, Tech. rep. Dübendorf, Switzerland: Empa, Swiss Federal Laboratories for Materials Science and Technology. Available at: https://www.empa.ch/documents/56101/617885/FR_Smartcarb_final_Jan2019.pdf (Accessed September 23, 2019).

LandGEM. 2005. Available at https://www.epa.gov/catc/clean-air-technology-center-products#software. Accessed August 18, 2019.

Liu, Z, He, C, Zhou, Y and **Wu, J.** 2014. How much of the world's land has been urbanized, really? A hierarchical framework for avoiding confusion. *Landscape Ecol* **29**(5): 763–771. DOI: https://doi.org/10.1007/s10980-014-0034-y

Mahadevan, P, Wofsy, SC, Matross, DM, Xiao, X, Dunn, AL, Lin, JC, Gerbig, C, Munger, JW, Chow, VY and **Gottlieb, EW.** 2008. A satellite-based biosphere parameterization for net ecosystem CO_2 exchange: Vegetation Photosynthesis and Respiration Model (VPRM). *Global Biogeochem Cy* **22**(2). DOI: https://doi.org/10.1029/2006GB002735

Mallaun, C, Giez, A and **Baumann, R.** 2015. Calibration of 3-D wind measurements on a single-engine research aircraft. *Atmos Meas Tech* **8**(8): 3177–3196. DOI: https://doi.org/10.5194/amt-8-3177-2015

Marcotullio, PJ, Sarzynski, A, Albrecht, J, Schulz, N and **Garcia, J.** 2013. The geography of global urban greenhouse gas emissions: An exploratory analysis. *Climatic Change* **121**(4): 621–634. DOI: https://doi.org/10.1007/s10584-013-0977-z

Mays, KL, Shepson, PB, Stirm, BH, Karion, A, Sweeney, C and **Gurney, KR.** 2009. Aircraft-based measurements of the carbon footprint of Indianapolis. *Environ Sci Technol* **43**(20): 7816–7823. DOI: https://doi.org/10.1021/es901326b

McDonald, BC, McBride, ZC, Martin, EW and **Harley, RA.** 2014. High-resolution mapping of motor vehicle carbon dioxide emissions. *J Geophys Res-Atmos* **119**(9): 5283–5298. DOI: https://doi.org/10.1002/2013JD021219

Mertens, M and **Jöckel, P.** 2020. Data from MECO(n) model simulations on "Urban greenhouse gas emissions from the Berlin area: A case study using airborne CO_2 and CH_4 in situ observations in summer 2018". DOI: https://doi.org/10.5281/zenodo.3707990

Mertens, M, Kerkweg, A, Jöckel P, Tost, H and **Hofmann, C.** 2016. The 1-way on-line coupled model system MECO(n) – Part 4: Chemical evaluation (based on MESSy v2.52). *Geosci Model Dev* **9**: 3545–3567. DOI: https://doi.org/10.5194/gmd-9-3545-2016

MLUL. 2017. Available at https://mlul.brandenburg.de/cms/media.php/lbm1.a.3310.de/Lagebericht-Abwasserbeseitigung2017.pdf. Accessed August 18, 2019.

Mueller, K, Yadav, V, Lopez-Coto, I, Karion, A, Gourdji, S, Martin, C and **Whetstone, J.** 2018. Siting Background Towers to Characterize Incoming Air fro Urban Greenhouse Gas Estimation: A Case Study in the Washington, DC/Baltimore Area. *J Geophys Res Atmos* **123**(5): 2910–2926. DOI: https://doi.org/10.1002/2017JD027364

Nisbet, E and **Weiss, R.** 2010. Atmospheric science: Top-down versus bottom-up. *Science* **328**(5983): 1241–1243. DOI: https://doi.org/10.1126/science.1189936

OpenStreetMap. 2018. Available at http://download.geofabrik.de/europe/germany/berlin.html. Accessed Ocotber 02, 2019.

O'Shea, SJ, Allen, G, Fleming, ZL, Bauguitte, SJ-B, Percival, CJ, Gallagher, MW, Lee, J, Helfter, C and **Nemitz, E.** 2014. Area fluxes of carbon dioxide, methane, and carbon monoxide derived from airborne measurements around Greater London: A case study during summer 2012. *J Geophys Res-Atmos* **119**(8): 4940–4952. DOI: https://doi.org/10.1002/2013JD021269

Peischl, J, Ryerson, TB, Aikin, KC, de Gouw, JA, Gilman, JB, Holloway, JS, Lerner, BM, Nadkarni, R, Neuman, JA, Nowak, JB, Trainer, M, Warneke, C and **Parrish, DD.** 2015. Quantifying atmospheric methane emissions from the Haynesville, Fayetteville, and northeastern Marcellus shale gas production regions. *J Geophys Res-Atmos* **120**(5): 2119–2139. DOI: https://doi.org/10.1002/2014JD022697

Peischl, J, Ryerson, TB, Brioude, J, Aikin, KC, Andrews, AE, Atlas, E, Blake, D, Daube, BC, de Gouw, JA, Dlugokencky, E, Frost, GJ, Gentner, DR, Gilman, JB, Goldstein, AH, Harley, RA, Holloway, JS, Kofler, J, Kuster, WC, Lang, PM, Novelli, PC, Santoni, GW, Trainer, M, Wofsy, SC and **Parrish, DD.** 2013. Quantifying sources of methane using light alkanes in the Los Angeles basin, California. *J Geophys Res-Atmos* **118**(10): 4974–4990. DOI: https://doi.org/10.1002/jgrd.50413

Pillai, D, Buchwitz, M, Gerbig, C, Koch, T, Reuter, M, Bovensmann, H, Marshall, J and **Burrows, JP.** 2016. Tracking city CO_2 emissions from space using a high-resolution inverse modelling approach: A case study for Berlin, Germany. *Atmos Chem Phys* **16**(15): 9591–9610. DOI: https://doi.org/10.5194/acp-16-9591-2016

Pitt, JR, Allen, G, Bauguitte, SJ-B, Gallagher, MW, Lee, JD, Drysdale, W, Nelson, B, Manning, AJ and **Palmer, PI.** 2019. Assessing London CO_2, CH_4 and CO emissions using aircraft measurements and dispersion modelling. *Atmos Chem Phys* **19**(13): 8931–8945. DOI: https://doi.org/10.5194/acp-19-8931-2019

Plant, G, Kort, EA, Floerchinger, C, Gvakharia, A, Vimont, I and **Sweeney, C.** 2019. Large fugitive

methane emissions from urban centers along the US East Coast. *Geophys Res Lett* **46**(14): 8500–8507. DOI: https://doi.org/10.1029/2019GL082635

Ren, X, Salmon, OE, Hansford, JR, Ahn, D, Hall, D, Benish, SE, Stratton, PR, He, H, Sahu, S, Grimes, C, Heimburger, AMF, Martin, CR, Cohen, MD, Stunder, B, Salawitch, RJ, Ehrman, SH, Shepson, PB and **Dickerson, RR.** 2018. Methane Emissions From the Baltimore-Washington Area Based on Airborne Observations: Comparison to Emissions Inventories. *J Geophys Res-Atmos* **123**(16): 8869–8882. DOI: https://doi.org/10.1029/2018JD028851

Rockel, B, Will, A and **Hense, A.** 2008. The regional climate model COSMO-CLM (CCLM). *Meteorol Z* **17**: 347–348. DOI: https://doi.org/10.1127/0941-2948/2008/0309

Saunois, M, Bousquet, P, Poulter, B, Peregon, A, Ciais, P, Canadell, JG, Dlugokencky, EJ, Etiope, G, Bastviken, D, Houweling, S, Janssens-Maenhout, G, Tubiello, FN, Castaldi, S, Jackson, RB, Alexe, M, Arora, VK, Beerling, DJ, Bergamaschi, P, Blake, DR, Brailsford, G, Brovkin, V, Bruhwiler, L, Crevoisier, C, Crill, P, Covey, K, Curry, C, Frankenberg, C, Gedney, N, Höglund-Isaksson, L, Ishizawa, M, Ito, A, Joos, F, Kim, H-S, Kleinen, T, Krummel, P, Lamarque, J-F, Langenfelds, R, Locatelli, R, Machida, T, Maksyutov, S, McDonald, KC, Marshall, J, Melton, JR, Morino, I, Naik, V, O'Doherty, S, Parmentier, F-JW, Patra, PK, Peng, C, Peng, S, Peters, GP, Pison, I, Prigent, C, Prinn, R, Ramonet, M, Riley, WJ, Saito, M, Santini, M, Schroeder, R, Simpson, IJ, Spahni, R, Steele, P, Takizawa, A, Thornton, BF, Tian, H, Tohjima, Y, Viovy, N, Voulgarakis, A, van Weele, M, van der Werf, GR, Weiss, R, Wiedinmyer, C, Wilton, DJ, Wiltshire, A, Worthy, D, Wunch, D, Xu, X, Yoshida, Y, Zhang, B, Zhang, Z and **Zhu, Q.** 2016. The global methane budget 2000–2012. *Earth Syst Sci Data* **8**(2): 697–751. DOI: https://doi.org/10.5194/essd-8-697-2016

Saunois, M, Bousquet, P, Poulter, B, Peregon, A, Ciais, P, Canadell, JG, Dlugokencky, EJ, Etiope, G, Bastviken, D, Houweling, S, Janssens-Maenhout, G, Tubiello, FN, Castaldi, S, Jackson, RB, Alexe, M, Arora, VK, Beerling, DJ, Bergamaschi, P, Blake, DR, Brailsford, G, Bruhwiler, L, Crevoisier, C, Crill, P, Covey, K, Frankenberg, C, Gedney, N, Höglund-Isaksson, L, Ishizawa, M, Ito, A, Joos, F, Kim, H-S, Kleinen, T, Krummel, P, Lamarque, J-F, Langenfelds, R, Locatelli, R, Machida, T, Maksyutov, S, Melton, JR, Morino, I, Naik, V, O'Doherty, S, Parmentier, F-JW, Patra, PK, Peng, C, Peng, S, Peters, GP, Pison, I, Prinn, R, Ramonet, M, Riley, WJ, Saito, M, Santini, M, Schroeder, R, Simpson, IJ, Spahni, R, Takizawa, A, Thornton, BF, Tian, H, Tohjima, Y, Viovy, N, Voulgarakis, A, Weiss, R, Wilton, DJ, Wiltshire, A, Worthy, D, Wunch, D, Xu, X, Yoshida, Y, Zhang, B, Zhang, Z and **Zhu, Q.** 2017. Variability and quasi-decadal changes in the methane budget over the period 2000–2012. *Atmos Chem Phys* **17**(18): 11135–11161. DOI: https://doi.org/10.5194/acp-17-11135-2017

Scherer, D, Ament, F, Emeis, S, Fehrenbach, U, Leitl, B, Scherber, K, Schneider, C and **Vogt, U.** 2019a. Three-Dimensional Observation of Atmospheric Processes in Cities. *Meteorol Z* **28**(2): 121–138. DOI: https://doi.org/10.1127/metz/2019/0911

Scherer, D, Antretter, F, Bender, S, Cortekar, J, Emeis, S, Fehrenbach, U, Gross, G, Halbig, G, Hasse, J, Maronga, B, Raasch, S and **Scherber, K.** 2019b. Urban Climate Under Change [UC]^2 – A National Research Programme for Developing a Building-Resolving Atmospheric Model for Entire City Regions. *Meteorol Z* **28**(2): 95–104. DOI: https://doi.org/10.1127/metz/2019/0913

Statistisches Bundesamt. 2018. Available at www.destatis.de/DE/Themen/Laender-Regionen/Regionales/Gemeindeverzeichnis/Administrativ/05-staedte.html. Accessed September 25, 2019.

Stein, AF, Draxler, RR, Rolph, GD, Stunder, BJB, Cohen, MD and **Ngan, F.** 2015. NOAA's HYSPLIT atmospheric transport and dispersion modeling system. *Bull Amer Meteor Soc* **96**: 2059–2077. DOI: https://doi.org/10.1175/BAMS-D-14-00110.1

Stohl, A. 1998. Computation, accuracy and applications of trajectories – A review and bibliography. *Atmospheric Environment* **32**(6): 947–966. DOI: https://doi.org/10.1016/S1352-2310(97)00457-3

Strukturatlas Land Brandenburg. 2017. Plot received from an interactive tool on http://strukturatlas.brandenburg.de/. Accessed January 22, 2020.

Turnbull, JC, Karion, A, Davis, K, Lauvaux, T, Miles, NL, Richardson, SJ, Sweeney, C, McKain, K, Lehman, SJ, Gurney, KR, Patarasuk, R, Liang J, Shepson, PB, Heimburger, A, Harvey, Rand **Whetstone, J.** 2019. Synthesis of Urban CO_2 Emission Estimates from Multiple Methods from the Indianapolis Flux Project (INFLUX). *Environmental science & technology* **53**(1): 287–295. DOI: https://doi.org/10.1021/acs.est.8b05552

UN. 2018. World Urbanization Prospects 2018. Available at https://population.un.org/wup/Publications/. Accessed September 25, 2019.

UNFCCC. 2015. Paris Agreement, FCCC/CP/2015/L.9/Rev.1. Available at https://unfccc.int/resource/docs/2015/cop21/eng/l09r01.pdf. Accessed September 25, 2019.

Zhao, CL and **Tans, PP.** 2006. Estimating uncertainty of the WMO mole fraction scale for carbon dioxide in air. *J Geophys Res* **111**(D8): 81. DOI: https://doi.org/10.1029/2005JD006003

Zimnoch, M, Necki, J, Chmura, L, Jasek, A, Jelen, D, Galkowski, M, Kuc, T, Gorczyca, Z, Bartyzel, J and **Rozanski, K.** 2019. Quantification of carbon dioxide and methane emissions in urban areas: Source apportionment based on atmospheric observations. *Mitig Adapt Strat Gl* **24**(6): 1051–1071. DOI: https://doi.org/10.1007/s11027-018-9821-0

How to cite this article: Klausner, T, Mertens, M, Huntrieser, H, Galkowski, M, Kuhlmann, G, Baumann, R, Fiehn, A, Jöckel, P, Pühl, M and Roiger, A. 2020. Urban greenhouse gas emissions from the Berlin area: A case study using airborne CO_2 and CH_4 in situ observations in summer 2018. *Elem Sci Anth,* 8: 15. DOI: https://doi.org/10.1525/elementa.411

Domain Editor-in-Chief: Detlev Helmig, Institute of Alpine and Arctic Research, University of Colorado Boulder, US

Associate Editor: Lori Bruhwiler, Global Monitoring Division, NOAA Earth System Research Laboratory, US

Knowledge Domain: Atmospheric Science

Submitted: 12 November 2019 **Accepted:** 19 March 2020 **Published:** 16 April 2020

ELEMENTA Science of the Anthropocene

Elem Sci Anth is a peer-reviewed open access journal published by University of California Press.

OPEN ACCESS